DESIGN AND ANALYSIS OF A PARABOLIC TROUGH SOLAR CONCENTRATOR

A Thesis
presented to
the Faculty of California Polytechnic State University,
San Luis Obispo

In Partial Fulfillment
of the Requirements for the Degree
Master of Science in Civil and Environmental Engineering

By
George Nicholas Skouras
August 2018

COMMITTEE MEMBERSHIP

TITLE:	Design and Analysis of a Parabolic Trough Solar Concentrator
AUTHOR:	George Nicholas Skouras
DATE SUBMITTED:	August 2018
COMMITTEE CHAIR:	Rebekah Oulton, Ph.D., PE Assistant Professor of Water Resources
COMMITTEE MEMBER:	Tryg Lundquist, Ph.D. Professor of Environmental Engineering
COMMITTEE MEMBER:	Yarrow Nelson, Ph.D. Professor of Environmental Engineering

ABSTRACT

Design and Analysis of a Parabolic Trough Solar Concentrator

George Nicholas Skouras

A prototype solar desalination system (SODESAL) with a parabolic-trough solar concentrator (PTSC) and evacuated tube was designed and analyzed to determine the solar thermal capabilities for small-scale distillation and energy generation. A proof-of-concept study verified that distillation is possible with the system as designed, however a rupture occurred in the copper heat-pipe heat exchanger due to overheating. The internal temperatures of an aluminum heat transfer fin were measured inside an evacuated tube typically used in solar water heater systems to understand the lateral heat distribution and identify possible causes of the rupture. Solar radiation was measured for both the summer and winter solstices to understand the relationship between incident solar radiation and the potential freshwater yield of the system. The lateral heat distribution of the AHTF is dependent upon the PTSC's solar incident angle. A consistent lateral heat distribution occurred across the AHTF approximately 40 mins after solar noon. The temperature difference between each end of the AHTF can exceed over 225 °C leading up to and following solar noon when the PTSC was set at a static slope. The SODESAL system's future applications, system improvements and additional research are also discussed along with the capability of small-scale CSP systems.

Keywords: Solar Desalination, Parabolic Trough Solar Concentrator

ACKNOWLEDGMENTS

I would like to thank everyone who has helped me and supported me in this endeavor. My advisor, Dr. Rebekah Oulton, has spent the last three years supporting me and encouraging me for which I am very thankful. I would also like to thank Dr. Yarrow Nelson for convincing me to pursue a future at Cal Poly when I was only a prospective student many years ago. Your passion for environmental engineering had a profound impact on my desire to continue my graduate education for which am a very grateful. Thank you to Dr. Tryg Lundquist for instructing me over the last three years of graduate school, it was truly a pleasure to be in your classes especially on Fridays. I would like to thank Teyvon Brooks for his help in designing my system and the countless hours we spent late at night building, testing and ultimately succeeding with the project. Thank you to the Cal Poly Machine Shop Technicians for your expertise and guidance through fabrication, I would have been lost without all your help. I would like to thank the Cal Poly Student Fee Initiative Committee, without your financial support my project would not be possible and for which I am very thankful. I would also like to thank the many undergraduates who worked on this project. Your hard work and dedication motivated me more than you can imagine, and I hope my project inspired you to pursue your own goals no matter how daunting they may seem. I would like to thank my family and friends for their support and unwavering patience during my education. I could not have completed this project without your help and I graciously appreciate all the time and resources you sacrificed for me.

TABLE OF CONTENTS

LIST OF TABLES

LIST OF FIGURES

1. INTRODUCTION

Water is one of the most essential resources to support the Earth's ecosystems and human civilization. Most of the water present on the planet is saltwater, and only a small portion is available as freshwater [1]. Agriculture, industry, power generation, sanitation and direct consumption all depend on reliable freshwater resources to function. A rise in developing nations and human population will further increase the demand for freshwater resources at a rate which the natural world cannot support.

The effects of climate change include shifting rainfall patterns and disrupting the natural hydrologic cycle of regenerating freshwater resources. As more evidence supports the causality of climate change occurring from human consumption of fossil fuels, water-scarce areas should develop sustainable solutions for acquiring freshwater that are fossil-fuel free. Desalination is a well-practiced solution for removing dissolved solids from seawater to produce freshwater for coastal regions that have access to inexpensive electricity [20]. The most common method for desalination is reverse osmosis (RO) which can purify seawater into potable water; however, RO systems are expensive to maintain and require a high energy input and extensive energy infrastructure to operate. Some developing countries do not have the resources or infrastructure available to develop and operate RO systems. However, sunlight is an abundant and reliable resource which can provide developing countries with the necessary energy to purify saltwater to provide for their freshwater needs.

Solar power generation technologies have improved over the last decade, especially for concentrated solar power (CSP) systems [15]. CSP systems typically utilize a parabolic trough solar collector (PTSC) in an array field for large-scale electrical power generation [12]. The

collector's parabolic shape concentrates sunlight onto a cylindrical absorber located at the parabola's focal point. The heat generated at the focal point is used to produce steam for electrical power [20].

CSP technology is also capable of treating saltwater directly, by distilling the generated steam into freshwater [20]. Pilot-scale CSP desalination systems have successfully demonstrated their capability to recycle agricultural run-off with high salinities [22]. Small-scale solar desalination systems (SODESAL) also have the potential to provide freshwater solutions for deployment for disaster relief, permanent off-grid recycled water, residential and communal potable water and seawater purification. The concentrated sunlight is converted into thermal energy which heats a heat transfer fluid and loops through a steam generator. The generated steam is passed through a multi-effect distillation system which recycles the latent heat of the distillate to heat incoming feed water and improve the system's overall efficiency [22]. These types of solar-powered desalination systems can treat high-salinity waters such as seawater, brackish water and wastewater and have the potential to produce a zero-liquid discharge for solids recovery[22].

Solar powered desalination systems may play a key role in the future to maximize the yield of recycled water without adding fossil fuel demand. Significant developments have been made in improving the efficiencies and yields of small-scale solar desalination [25]. Current technology allows small-scale systems to operate with similar thermal characteristics as large-scale solar powered systems with comparable internal temperatures generated along the focal point of the PTSC [15].

The research herein explores the capabilities of a small-scale PTSC for application in a solar thermal desalination system. A prototype PTSC system was designed and constructed to be capable of several methods of solar tracking. A proof-of-concept study verified that distillation is possible with the system as designed. The internal temperatures of an aluminum heat transfer fin were measured inside an evacuated tube to understand the lateral heat distribution due to an overheating rupture during early testing. Solar radiation was measured for both the summer and winter solstices to understand the relationship between incident solar radiation and the potential thermal output of the system.

2. BACKGROUND

Freshwater resources only account for 2.5% of the total water on earth; the remainder is comprised of ocean and saline water. Only approximately 30% of freshwater is accessible for direct use by humans in the form of groundwater, lakes, rivers and other surfaces waters [1]. This means the majority of global freshwater is locked in glaciers, icecaps and permafrost. Solar technologies have long been used to address a variety of societal needs, and these technologies have potential to help address the challenge of increasing societal demand for these limited freshwater resources. This study focuses on how solar technologies can improve desalination options to meet these demands and the growing capabilities of small-scale SODESAL systems.

2.1 Global Water Footprint

Identifying the water footprint of a nation is an effective way to understand the nation's water demands. The water footprint is defined as the volume of water needed to produce goods and services consumed by the inhabitants of the country. The water footprint also includes virtual water costs which is water associated with manufacturing or producing a product that is traded between nations [2].

There are four main factors that contribute to a high-water footprint:

- The total volume of consumption, which is generally related to gross national income of a country. Richer countries can afford more access to water, so their footprint is typically higher.
- Water-intensive activities like producing livestock for meat consumption. Producing meat and other livestock lowers the efficiency of water use as the chain of production moves upwards.

- The climate of the region. Areas with a hot climate have high amounts of evaporation and therefore a higher water footprint due to losses.
- Water-inefficient agricultural practices due to lack of adequate technology or the low yield of crops per amount of water used [2].

The global water footprint is estimated as 7450 Gm^3/year or about 1240 m^3/year per capita. The United States consumes the most water per capita (2480 m^3/year) whereas China consumes very little water per capita (700 m^3/year), as shown in Figure 2.1 [2]. Agriculture and food consumption contribute the largest portion of a nation's water footprint. The water footprint for global agriculture is 6,390 Gm^3/year; if irrigation losses are included the total global footprint for agriculture increases to 7980 Gm^3/year [2].

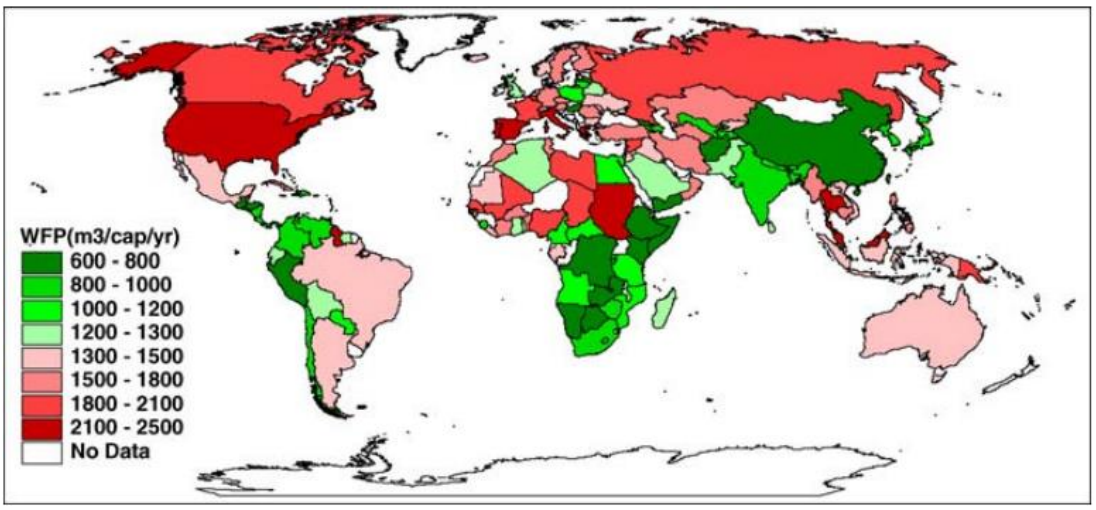

Figure 2.1: Average National Water Footprints per Capita (m^3/capita/year) [2]

2.2 Solar Radiation Resource

Solar radiation arrives from the sun and is expressed by a value called the solar constant. The exact value of the solar constant varies throughout the year due to the eccentricity of the Earth's orbit; however, the World Radiation Center (WRC) has adopted a standard value of 1367

W/m^2 [3]. Solar radiation is comprised of two major components, beam radiation and diffuse radiation. Their sum on a horizontal surface is called the total solar radiation.

The units of solar radiation can be expressed in different ways. Instantaneous radiation is described by W/m^2 incident on a collector surface. The daily, monthly or yearly solar radiation is described by kWh/m^2/time and represents the average potential total solar radiation for a specific location or region [3].

2.2.1 Beam Radiation

Beam radiation, also referred to as direct solar radiation or direct normal irradiance (DNI), is solar radiation received on a surface normal to the position of the sun without having been scattered by the atmosphere [3, 4]. Beam radiation is especially important for solar concentrators since only beam radiation can be reflected for concentration. The global DNI resources for the world and the United States are shown in Figure 2.2 and Figure 2.3, respectively.

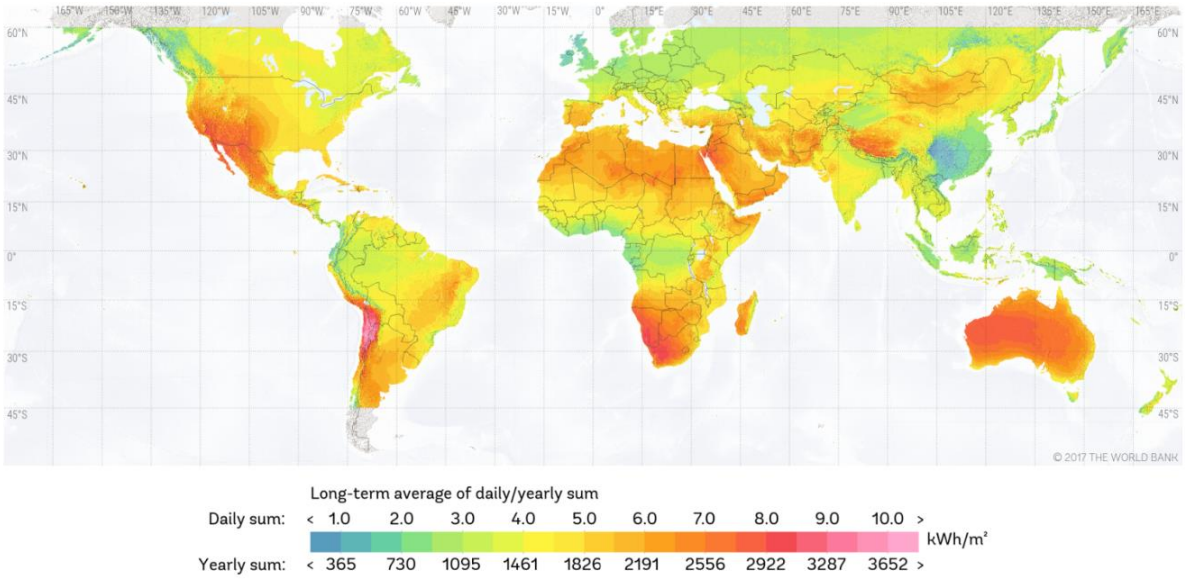

Figure 2.1: Global Direct Normal Irradiance [5]

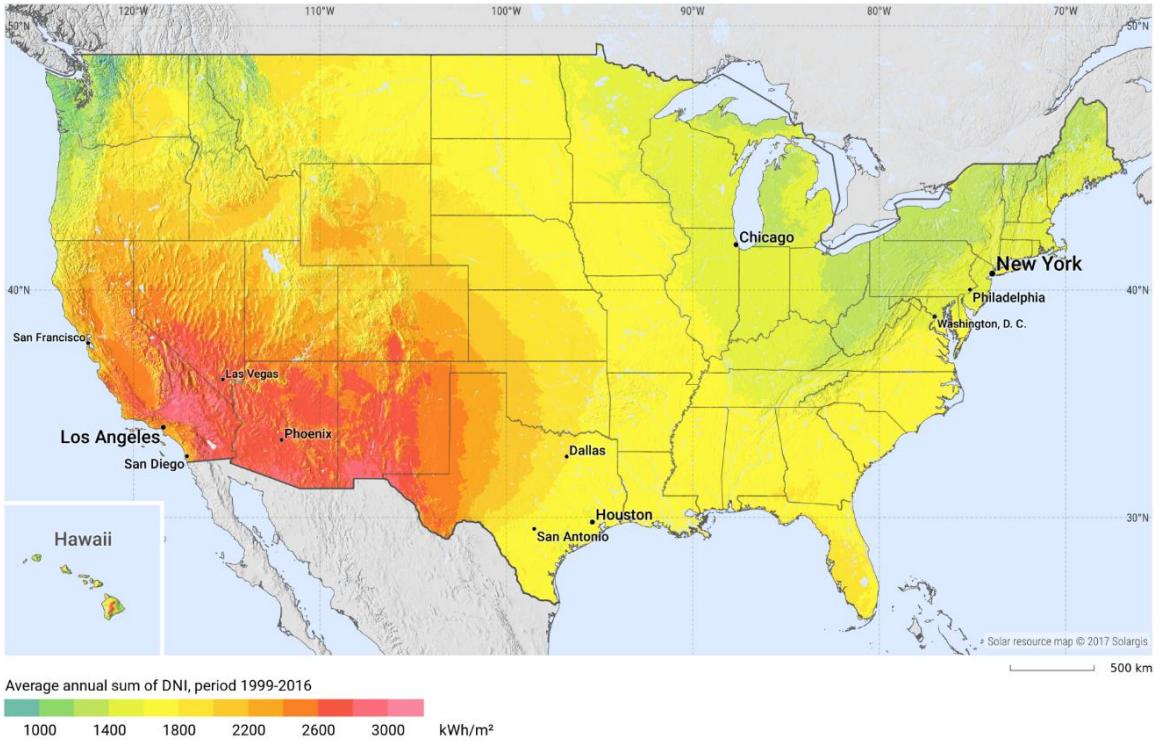

Figure 2.2: Direct Normal Irradiance for United States [6]

The average multi-year DNI for the Cal Poly test location was 6.84 (kWh/m^2/day) and is averaged from 1998-2015 data. The DNI was found using the National Renewable Energy Laboratory (NREL) Solar Prospector tool and is shown in Figure 2.4.

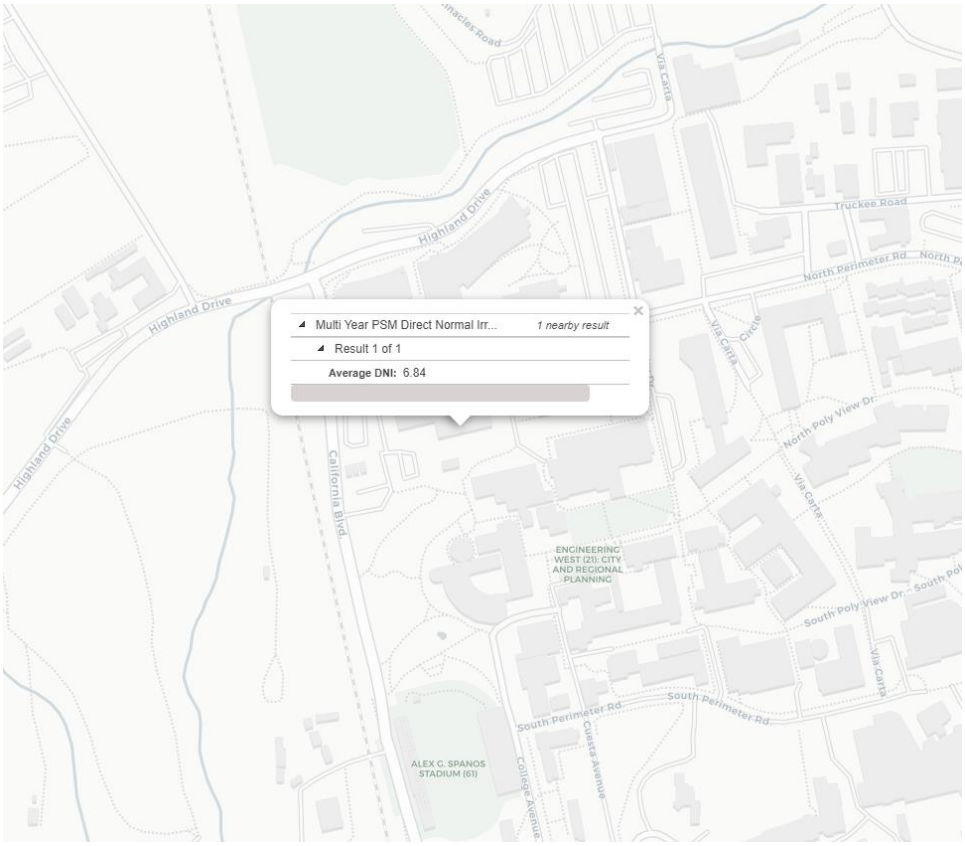

Figure 2.3: Direct Normal Irradiation for Cal Poly Test Location - San Luis Obispo, California [7]

2.2.2 Diffuse Radiation

Diffuse radiation, also referred to as Diffuse Horizontal Irradiance (DHI), is the radiation per unit area of a collector's surface received from the sun after its direction as been altered by colliding with molecules in the atmosphere. DHI is not subject to shade or shadows and comes equally from all directions (Figure 2.5) [3,4].

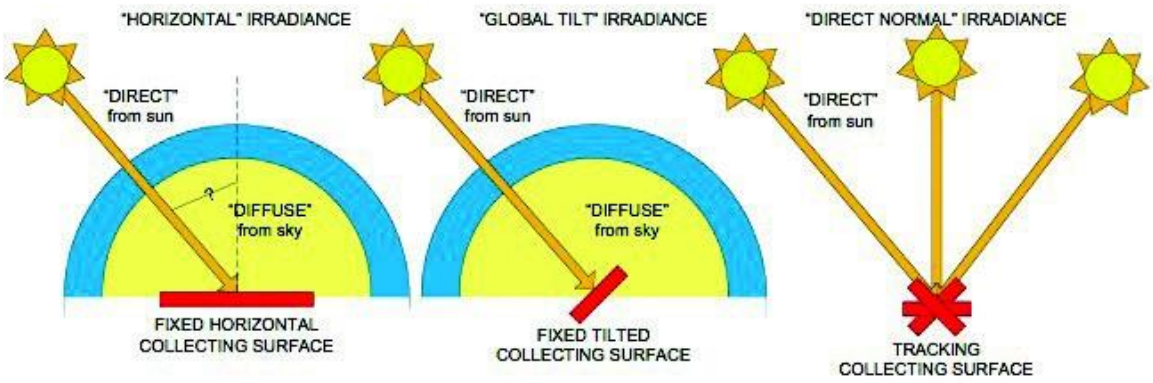

Figure 2.4: Horizontal Irradiance, Global Tilt Irradiance and Direct Normal Irradiance [4]

2.2.3 Total Solar Radiation

The total solar radiation, also known as the Global Horizontal Irradiance (GHI) is the sum of the direct normal irradiation and the diffuse solar radiation on a horizontal surface. The GHI is typically used to evaluate solar resources for energy generation since both forms of irradiation are used in photovoltaic systems [3, 4]. The global GHI values for the world and the United States are shown in Figure 2.6 and Figure 2.7, respectively.

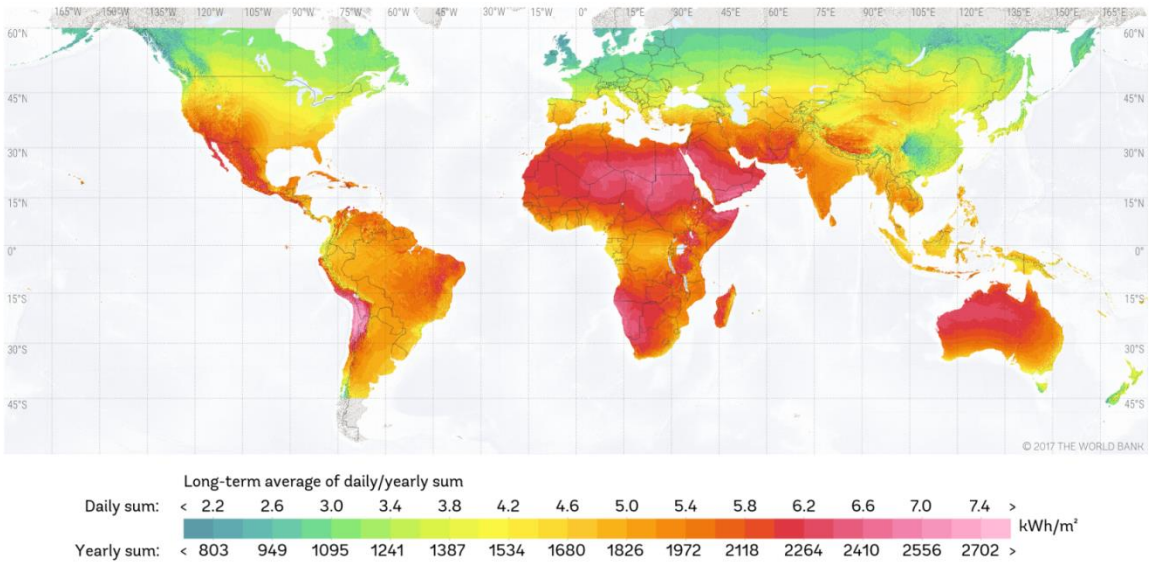

Figure 2.5: Global Horizontal Irradiation for World [8]

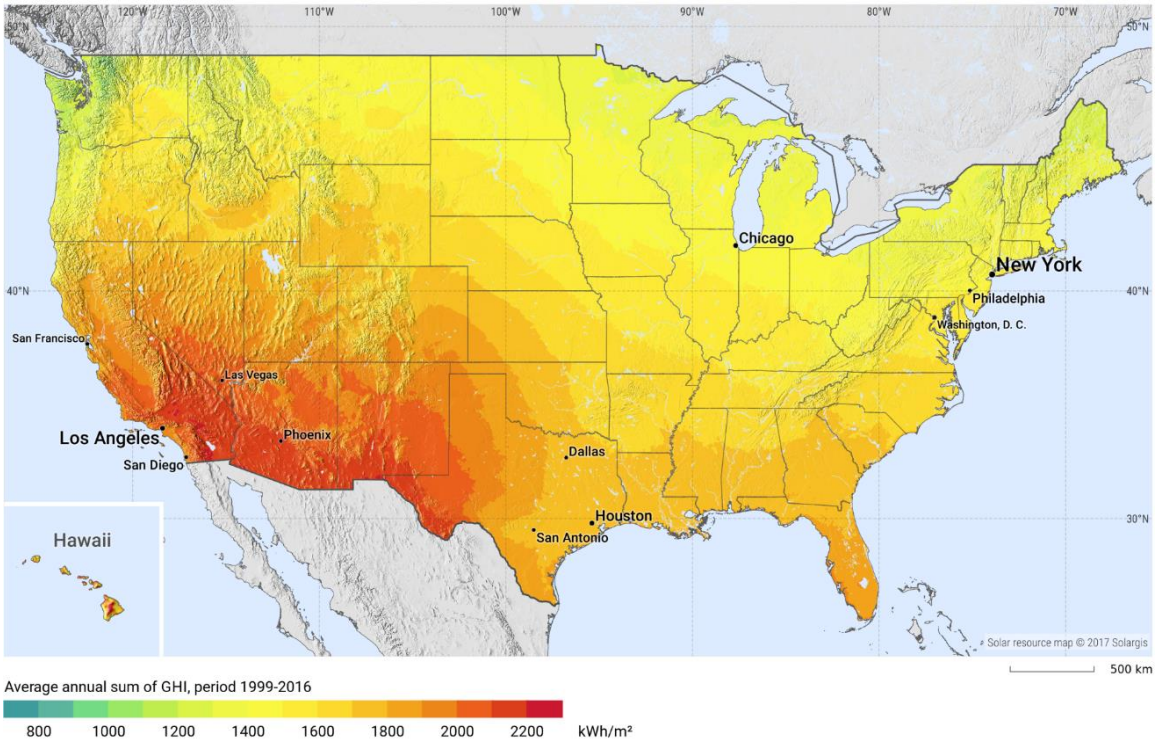

Figure 2.6: Global Horizontal Irradiation for United States [9]

2.3 Concentrated Solar Power

Concentrated solar power systems have been used throughout history to harness sunlight and generate solar thermal energy. Solar energy is concentrated when sunlight reflects off a parabolic surface onto a cylindrical surface located at the collector's focal point. A similar visualization of this concept is focusing sunlight with a magnifying glass. At a specific length away from the target, the optical properties of the lens align with the sun's incident rays and the focused image of light hits the surface, dramatically increasing the surface temperature.

2.3.1 History of Concentrated Solar Power

Harnessing the sun in this way can be dated back to the Greek scientist Archimedes (282-212 B.C.) reportedly using sunlight to burn invading Roman ships, Figure 2.8 [10].

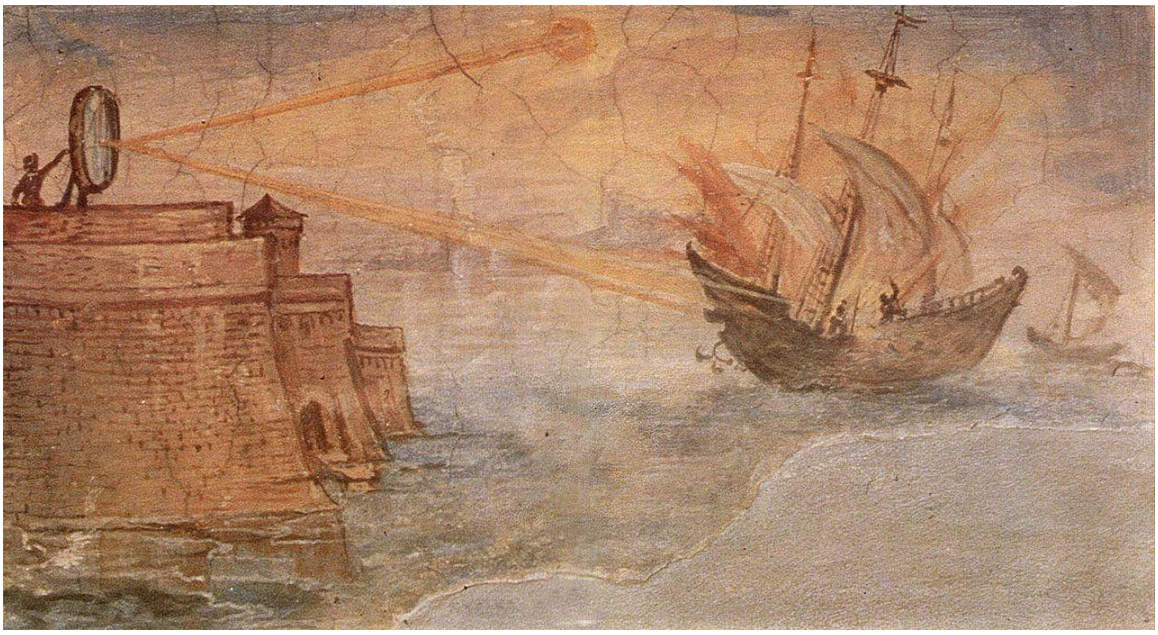

Figure 2.8: Archimedes' mirror used to burn Roman ships [10]

From 1852-1871, Augustin Mouchot taught secondary school mathematics during which he experimented on the conversion of solar energy into useful work. Mouchot's solar power designs were so successful he gained the support of the French government to pursue the research full-time. Mouchot's most inspiring device was demonstrated at the 1878 Universal Exhibition in Paris (Figure 2.9).

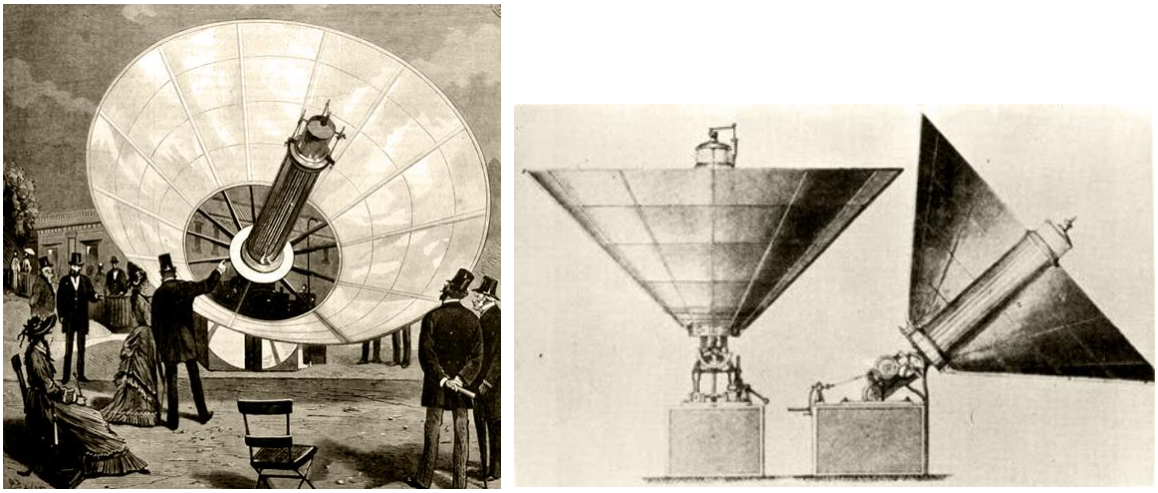

Figure 2.9: Augustin Mouchot's Solar Concentrator at the Universal Exhibition in Paris, 1878 [11]

Due to the falling price of coal and efficient trade agreements with Britain, Mouchot's work was seen as unnecessary and his funding was cut after the exhibition [11]. Mouchot's assistant, Abel Pifre continued his work and showcased a solar powered printing press in the Jardin des Tuileries in 1882. Even with cloudy conditions, the press was able to print 500 copies per hour, demonstrating the ability of solar concentrators to produce low pressure steam for a working steam engine (Figure 2.10) [11].

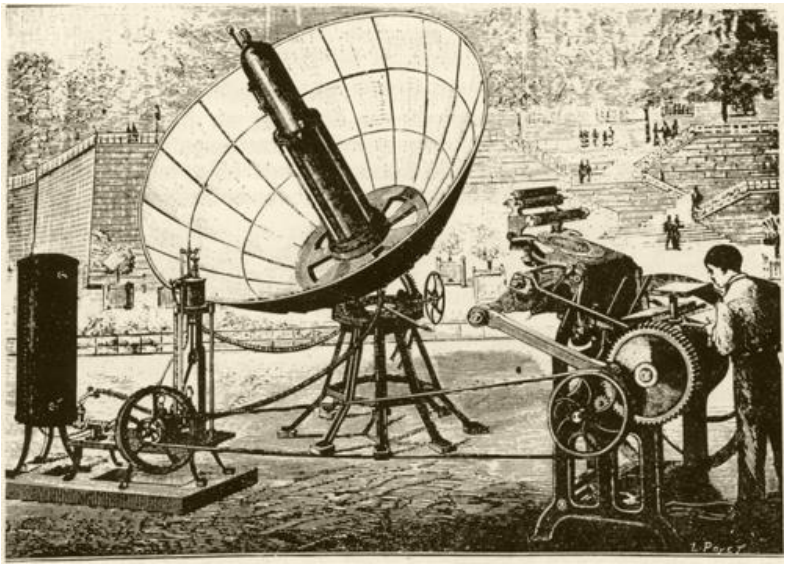

Figure 2.10: Abel Pifre and his solar powered printing press, 1882 [11]

During the 1870s and 1880s, the inventor and engineer John Ericsson developed a solar powered heat engine capable of combined operation with a conventional gas fuel source (Figure 2.11) [11].

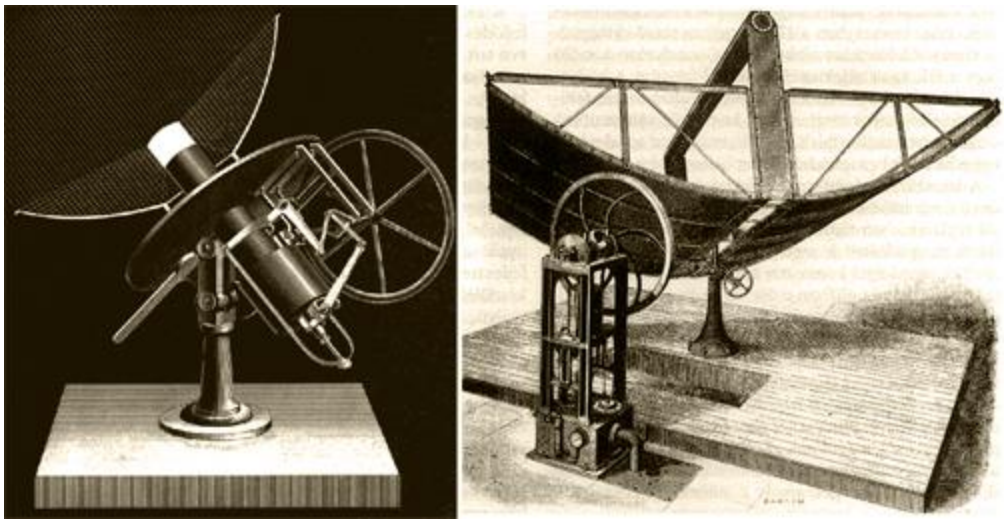

Figure 2.11: John Ericsson's Solar Engines [11].

Both Mouchot and Ericsson helped pioneer concentrated solar power as a renewable energy source. They realized that fossil fuel power was a finite resource and eventually the world would need to explore solar power as an alternative and sustainable solution for energy generation. The works of Mouchot, Pifre and Ericsson helped inspire future scientists to design the modern CSP systems in use today.

2.3.2 Modern Concentrated Solar Power Plants

Modern CSP power plants use highly reflective surfaces to concentrate and focus sunlight onto a receiver. These power plants consist of two parts, one that collects solar energy and converts it into heat, and another that converts the heat energy into electricity. Commercial CSP plants have operated in the United States for more than 15 years and require large areas to collect solar radiation for electricity production [12]. There are three types of CSP plants: parabolic trough systems, power towers and dish engine systems.

2.3.3 Parabolic Trough Power System

Parabolic trough systems consist of a parabolic mirror with a cylindrical receiver that contains an oil-filled pipe along the focal point of the solar concentrator (Figure 2.12). The mirror tracks the sun along one axis and heats an oil in the receiving tube to about 400°C which is used to boil water at high temperatures and pressure, producing superheated steam for a conventional steam turbine and generator (Figure 2.13) [12].

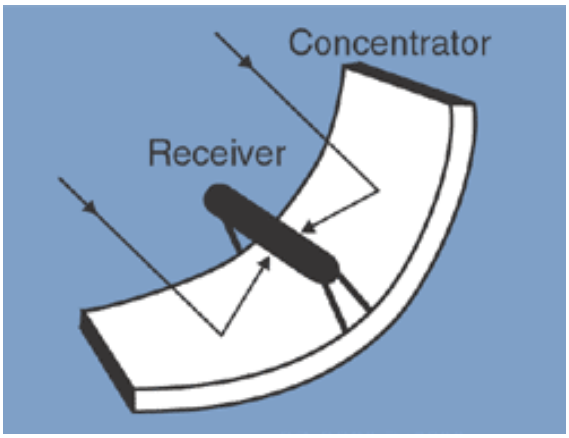

Figure 2.12: Parabolic Trough System Diagram [12]

Figure 2.13: Parabolic Trough System Array [12]

2.3.4 Power Tower System

Power towers, also known as central receivers, utilize many large flat heliostats to track the sun and focus incident rays onto a receiver. The receiver is located on top of a tower where concentrated sunlight heats a fluid like molten salt as hot as 570°C (Figures 2.14 & 2.15) [12].

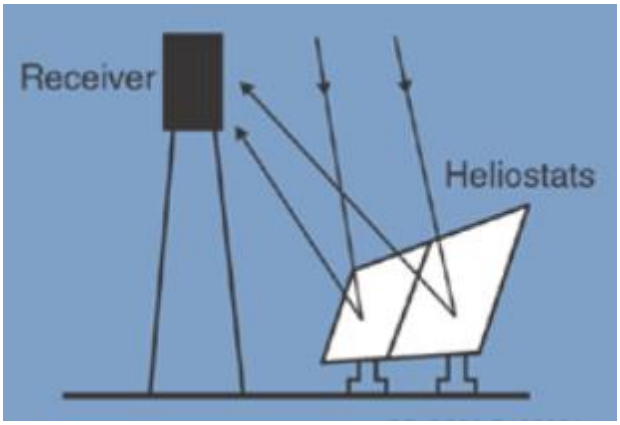

Figure 2.14: Power Tower System Diagram [12]

Figure 2.15: Power Tower [13]

The molten salt can retain heat exceptionally well making the system capable of storing thermal heat for days later to make steam for electricity generation. The thermal storage of these systems allows for electricity generation to continue even after sunset or when limited sunlight is available [13].

2.3.5 Dish-Engine System

Dish engine systems use a mirrored dish like the shape of a satellite dish to focus and concentrate sunlight onto a receiver. The dish tracks the sun's position in the sky in multiple axes and is typically coupled with a high-efficiency solar engine. The engine contains tubes filled with hydrogen or helium gas that help drive piston cylinders. The concentrated sunlight heats the gas in the cylinders, causing it to expand and drive the pistons. The pistons turn a crankshaft which drives an electric generator. The receiver, engine and generator are integrated and mounted at the focus of the dish (Figures 2.16 & 2.17) [12].

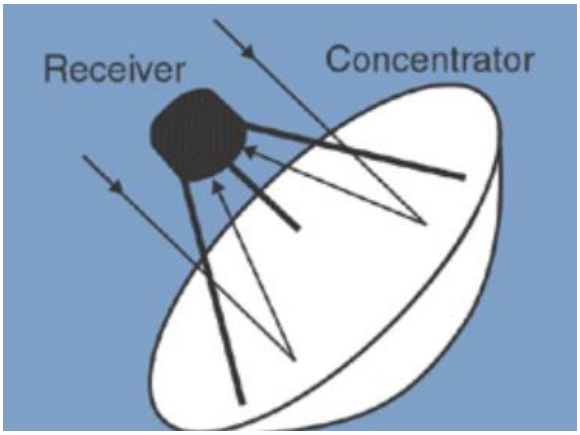

Figure 2.16: Dish-Engine System Diagram [12]

Figure 2.17: Solar Dish-Engine System [12]

2.3.6 CSP Global Market

About 90% of the global CSP market utilizes the parabolic trough collector system [14].

Spain added 400 MW of CSP plants in 2010 and is currently the global leader in CSP production with a total of 632 MW, compared to the United States with a total production of 509 MW [14].

There are several CSP power plants with unit capacities up to 80 MW in operation in United States and Spain (Figure 2.18) [15].

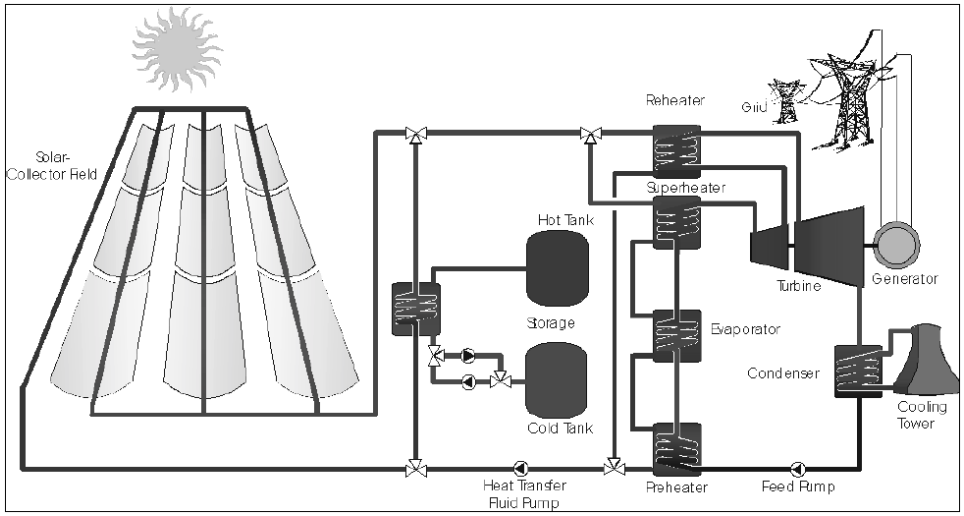

Figure 2.18: Linear Parabolic Trough Solar Collector Coupled to a Steam Cycle Power Station [15]

These systems predominantly track sunlight on the north-south axis and utilize a synthetic oil as a heat transfer fluid. The collectors can concentrate sunlight between 70-100 times normal radiation and typical operating temperatures are in the range of 350-550°C [15].

2.3.7 MENA CSP Potential

The Middle East and North African (MENA) region of the globe receives around 2400 kWh/m^2/year of solar energy; equivalent to 1.5 million barrels of crude oil per year for every square kilometer. A CSP plant the size of Lake Nasser, about 6000 km^2, would harvest the energy equivalent of the entire Middle East oil production, or about $9x10^9$ barrels per year [15]. Areas

with high solar insolation can meet the increasing demand for freshwater in water scarce regions of the world by providing a low-carbon energy supplement for desalination systems[19].

2.4 Desalination

Desalinated water is produced from either brackish water with salinity less than 10,000 mg/L or seawater with a salinity ranging between 30,000 to 44,000 mg/L and makes up 1% of the world's drinking water resources [21]. Over 50% over the world's population lives in urban centers bordering the ocean, and in many arid regions of the world like the Middle East, Australia, North Africa and Southern California, the population concentration along the coast exceeds 75% [21]. Desalination is expected to be an essential method to securing future water resources since the technique is drought-proof and has a nearly limitless supply [21].

Modern desalination consists of two basic methods for separating salts from ocean water: membrane separation and thermal distillation [20]. Reverse Osmosis (RO) membrane separation makes up about 60% of the world's desalination capacity. Saltwater is mechanically pressurized on one side of a membrane to force water molecules through a pore to remove particles greater than 0.1 nm. The resulting product water can have a total dissolved solids (TDS) content as low as 0 parts per million (ppm) [20]. Large-scale RO systems are ideally built adjacent to renewable energy resources such as solar power plants.

Thermal distillation occurs when saltwater is heated by steam to produce pure water vapor for condensation and ultimately consumption. The steam used to separate the pure water vapor from the saltwater is typically reused to improve the energy efficiency of the distillation system [20]. There are two types of thermal distillation: multistage flash distillation (MSF) and multi-

effect distillation (MED). Both MSF and MED processes can produce product water around 5-25 ppm TDS from seawater with TDS concentrations of 35,000 to 45,000 ppm [37].

MSF is the most commonly used thermal distillation method for treating seawater into freshwater. MSF is used for large capacity brine recirculation systems where typically low-pressure steam is recycled and used to flash-evaporate brine below the saturation vapor pressure in multiple stages. A portion of the saltwater is flashed into steam and the remaining brine is moved to the next flash stage. The flashed steam condenses and is collected as freshwater (Figure 2.19) [37].

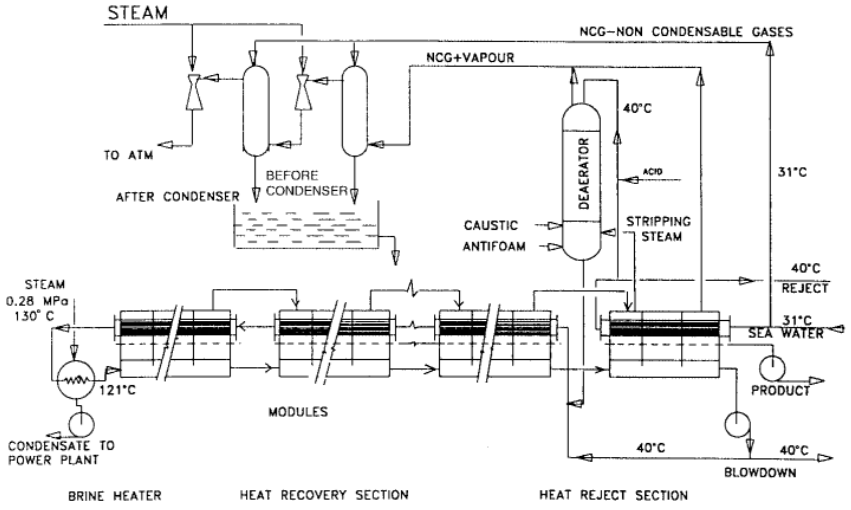

Figure 2.19: Schematic Flow Diagram of MSF distillation process with brine recirculation [37].

MED is a thermal distillation method where seawater is heated and processed in stages so that the latent heat from one stage is recycled and used in the next stage (Figure 2.20).

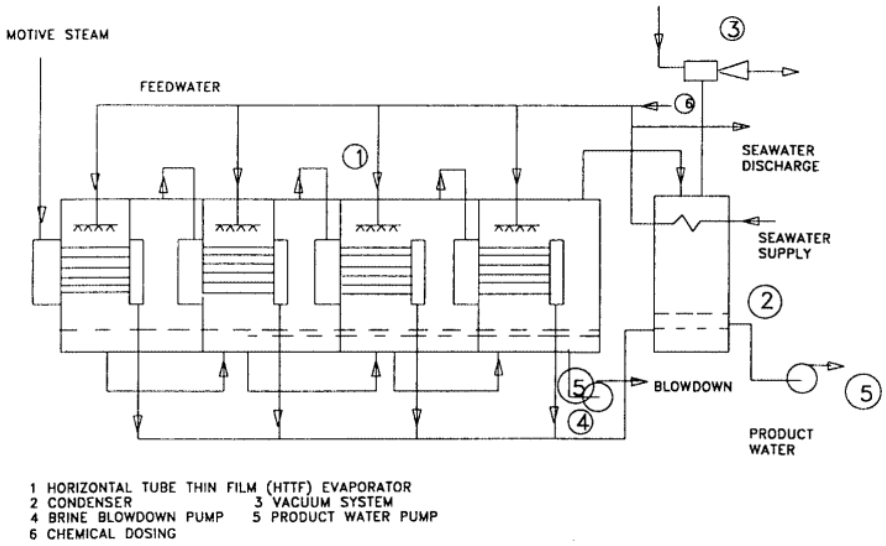

Figure 2.20: Schematic Flow Diagram of MED distillation process [37].

Incoming saltwater is heated by the first effect causing a fraction of the water to evaporate and condense on a heat transfer tube. The concentrated brine is sent to a 2nd effect where the internal pressure of the stage is lower. The vapor from the first effect condenses on a heat transfer tube in the second effect where the latent heat is used to generate almost an equal amount of vapor from the brine [37]. Each additional stage increases the thermal efficiency of the MED system [22].

2.4.1 Desalination Global market

Over the last 10 years, seawater reverse osmosis (SWRO) has dominated the desalination markets outside of the Middle East [21]. The Middle East has access to lower-cost fuel resources and many of its facilities co-generate power and water using CSP systems, which is why thermal distillation dominates the region [21]. At the end of 2015, there were 18,000 desalination plants worldwide with a total production capacity of 86,550,000 m^3/day [21]. Accelerated

development of desalination over the next decade is expected to be in Asia, the US and Latin America [21].

2.4.2 MENA Desalination

The MENA region is one of the most water scarce regions of the world, and some countries rely on desalination to either supplement or completely supply their freshwater resources (Figure 2.21) [16]. Desalination in the MENA region is projected to grow continuously at a rate of 7-9 % per year.

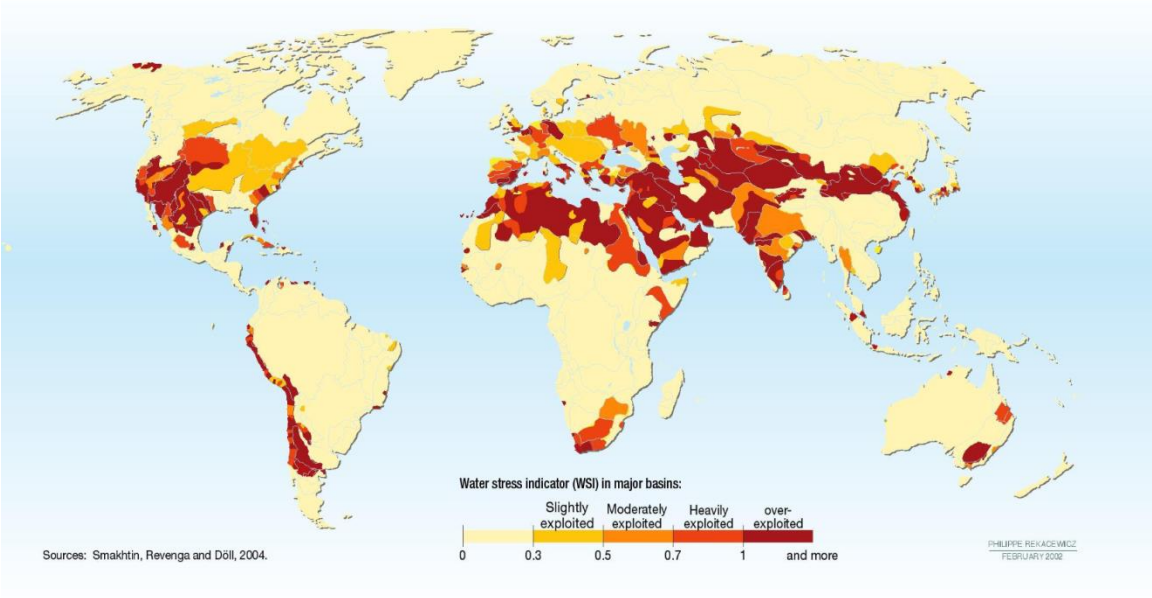

Figure 2.21: Global Water Scarcity Index [20]

Some of the top countries with seawater desalination plants are located within the MENA region, and their commissioned seawater desalination capacities are: Saudi Arabia (9,170,391 m^3/day), United Arab Emirates (8,381,299 m^3/day), Kuwait (2,586,761 m^3/day), Algeria (2,364,055 m^3/day) and Qatar (1,780,708 m^3/day) [17]. The total MENA region's desalination capacity is around 37,320,000 m^3/day [21]. As a comparison, the Carlsbad desalination plant in

California which is the largest seawater desalination plant on the western hemisphere, only produces 189,000 m^3/day [18].

2.4.3 Desalination Future Costs

Advances in technology are expected to reduce the cost of desalinated water by 20% in the next five years and by up to 60% in the next 20 years [21]. The cost of desalinated water in 2016 was \$0.80 - \$1.20/m^3 and is expected to drop to \$0.30 - \$0.50/m^3 within the next 20 years [21]. The reduction in costs for SWRO is attributed to advances in the membrane technology; the membranes are more productive due to higher surface areas and more densely packed membranes for the same individual membrane element [21]. The energy cost for SWRO desalination was reduced by 80% over the past 20 years. Presently, the energy required to produce freshwater from seawater for one household is about 2,000 kWh/year which is less energy than is used by a household's refrigerator [21].

2.4.4 Salinity

Feed water salinity plays a critical role in deciding which treatment technology to utilize for desalination. RO desalination requires greater energy per unit mass as the salinity of the feed water rises [20]. Salinity refers to the electrical conductivity of water and gives a bulk measurement of the total dissolves solids (TDS). The concentration of ions can be measured directly in µS/cm. Distilled water's conductivity can be between 0.5 to 3 µS/cm. Typical drinking water is anywhere below 100 µS/cm, and seawater can be as high as 54,000 µS/cm [20].

2.4.5 Scale Formation

The thermodynamic efficiency of a heat-transfer surface in thermal distillation is limited by the temperature that produces scale formation of the dissolved ions. Precipitation of scale-forming compounds is a complex relationship between temperature, pH, and the concentration of ions in the raw water upstream of the removal of water [20]. Seawater has two insoluble species that play a key role in the design temperature for the distillation system. Bicarbonate ions $(HCO_3)^-$ or alkaline scales begin to appear around 60°C in the form of soft scale or $CaCO_3$. Above 85°C the salt is predominantly $Mg(OH)_2$. The second type of salts is $CaSO_4$ and its hydrates, which can form hard scale at temperatures above 100°C. The addition of acids such as HCL or H_2SO_4 can help prevent scaling up to temperatures around 100°C, however their addition increases the risk of corrosion. Temperatures above 105 to 110°C make controlling scale formation difficult so most seawater desalination systems will generally not operate at those temperatures [20]. To overcome directly boiling seawater, distillation systems like MSF and MED use liquid films evaporating into a reduced pressure environment [20]. The top temperature range of thermal desalination systems with reduced pressure is typical between 60 to 100°C to reduce scaling

2.5 Previous CSP Studies

Pilot and small-scale CSP systems have been tested with the goal of maximizing the performance and understanding the ability to optimize these smaller systems into full size solar desalination systems. A good measure for a CSP system's thermal performance for desalination is the concentration ratio and the specific energy consumption of the system. The concentration ratio is a comparison between the collector's aperture area of sunlight concentrated onto the surface area of a receiver and is described in more detail in Section 3.2 [3]. The specific energy

consumption is a measure of how much thermal energy is required to produce a unit volume of product water [22]. Some systems will compare the price of generated power ($/watt) while other systems will compare the yield of freshwater in terms of (L/hr) or (kg/m^2·hr).

2.5.1 Solar Desalination Pilot Plant PTSC with MED-AHP

WaterFx® constructed and tested a pilot solar desalination system which desalinated agricultural runoff by using a parabolic trough solar collector (PTSC) coupled with an absorption heat pump (AHP) and a multi-effect distillation system (MED). According to the PTSC's manufacturer, SkyFuel®, the aperture area of the collector was 656 m^2 and the peak thermal efficiency was 73.7% based on 1000W/m^2 of solar irradiance [22]. The thermal efficiency is the system's ability to convert solar thermal energy into useable steam.

The heat transfer fluid used was Therminol XP, which is a food-grade mineral oil and was selected to reduce environmental hazards in the event of leakage [22]. The pilot system's MED had 3 effects for distillation, and each effect had its own recirculation pump and manual valve to control the recycle ratio for high-recovery experiments (Figure 2.22) [22].

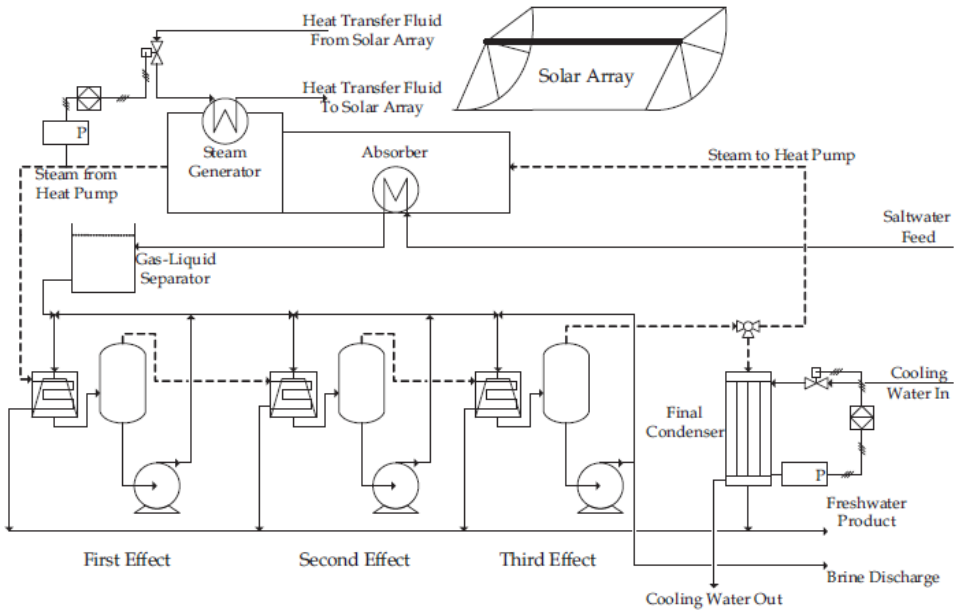

Figure 2.22: WaterFX® Process Flow Diagram [22].

The pilot study found that without the heat pump, the minimum distillation thermal energy consumption of the system was 261.87 kWh_{th}/m^3. With the absorption heat pump, the specific energy consumption was reduced to 133.2 kWh_{th}/m^3 [22]. The reduction in specific energy consumption can translate to a 49% reduction in solar array area required to power a process with the same freshwater production as a system with a similar adsorption heat pump [22].

The researchers also found that the most effective way to increase the instantaneous performance ratio (PR) and decrease the specific energy consumption (SC) of the MED is to increase the number of distillation effects in the system [22]. An optimized design was modeled using a 10-effect MED-AHP system which showed a specific energy consumption of 34.9 kWh_{th}/m^3 [22]. No degradation in overall system performance was measured due to scaling from a first-law perspective; however, there was measured degradation for the first distillation

effect's overall heat transfer coefficient. This degradation was recoverable with in-situ cleaning using an HCL acid wash [22].

2.5.2 Cal Poly San Luis Obispo CSP

Researchers from the Electrical Engineering Department at Cal Poly designed a low cost portable parabolic solar concentrator system to study the power and steam generation capability of a portable system (Figure 2.23). The team designed the solar concentrator's surface to create a low-cost and lightweight system that would still maintain durability and optical precision. The material for the mirror is a UV stabilized mirror finish on a thermoplastic backing that can withstand UV degradation for at least 10 years [23].

Figure 2.23: Cal Poly Prototype CSP System [23]

Tests were conducted to compare the performance in power output between vacuum insulated and uninsulated heat collecting pipes. The collector had an aperture area of 1.5 m^2 and was able to boil water for steam production at 170 W. The Cal Poly research yielded a price per watt of around $0.52/watt with a total project cost under $90 [23]. This experiment, although

simplified, demonstrated the ability to design a working small-scale CSP system with minimal capital cost.

2.5.3 Florida State University CSP Dish

The Florida State University's Sustainable Energy Science and Engineering Center (SESEC) program constructed an inexpensive parabolic dish concentrating system for electrical power generation and evaluation of overall system efficiency. The parabolic dish had a collector concentration ratio of 96 with an aperture area of 10.507m^2 (Figure 2.24) [24].

Figure 2.24: SESEC Parabolic Dish in Operation [24].

The constructed parabolic dish concentrator could theoretically produce temperatures to 712°C, however due to degradation of optics, maximum temperatures of approximately 560°C were achieved [24]. The solar radiation incident on the collector when these temperatures were measured was approximately 1064 W/m^2. The collector, steam turbine, and generator efficiencies were 95.56%, 49.98% and 16.42%, respectively. The energy conversion efficiency

from incoming solar energy to electric energy was 1.94%. The overall efficiency of the system was 7.3% [24].

One of the recommendations for improving a future design was utilizing a different material for the reflective surface of the parabolic mirror. The material used for this study was aluminized mylar which contained poor weathering characteristics.

2.5.4 Sharif University of Technology

Researchers at the Sharif University improved the thermal efficiency and yield production of a small-scale solar desalination system by adding oil inside an evacuated tube heat exchanger. The experimental design consisted of a single parabolic trough solar concentrator coupled with an evacuated heat pipe. Brackish water is inputted into a saltwater basin at specific water levels over a heat pipe. The steam generated in the basin is condensed in a corrugated tube and collected in a jar through a tube (Figure 2.25) [25].

Figure 2.25: Experimental Setup for Sharif University Desalination System [25]

The constructed system was oriented in the polar N-S axis to track the sun, with a system slope equal to the latitude of the location, approximately 35° N. As the collector rotated about the polar N-S axis, the incident angle is equal to the declination angle. The collector was rotated 15° an hour to maximize solar radiation on the absorber (Figure 2.26).

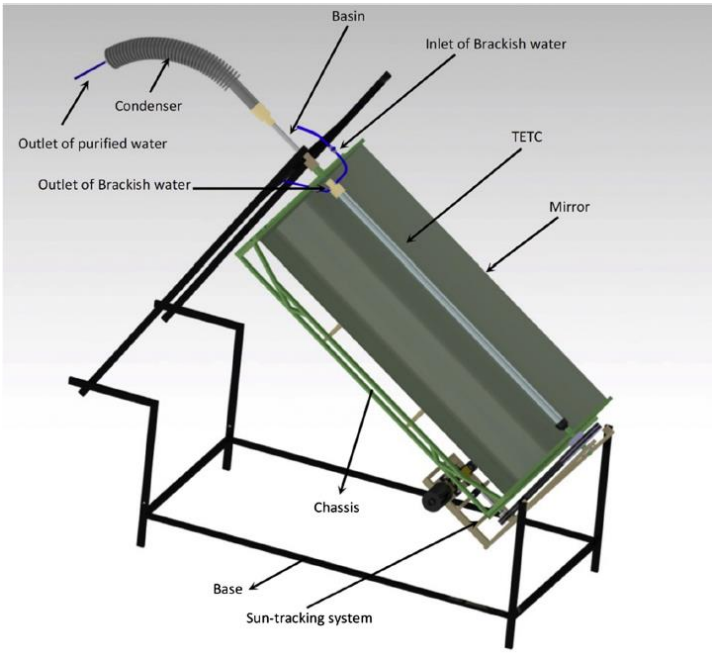

Figure 2.26: Schematic of Sharif University Solar Desalination System [25]

Multiple tests were conducted to investigate ways to improve the rate of freshwater production including the effect of water level in the saltwater basin and the use of different fluids inside the evacuated tube to improve thermal efficiency. The evacuated tube was filled with water and oil to increase the heat transfer rate between the pipe and the internal aluminum heat transfer fin[25].

The rate of production was highest for the oil filled evacuated tube due to the oil having a higher conductivity and therefore increasing heat transfer. The researchers concluded that the

increase in production rate was synchronous with the increase in solar intensity [25]. The maximum production rate for all three water volume fill levels occurred between 13:00 to 13:30 local time, which was synchronous with the maximum solar intensity [25]. Solar noon for the time of the study (August 2013) occurred around 13:39 local time [36]. This solar noon time was found using the longitude, latitude, and the local time and date for the experiment.

The maximum overall efficiency was 21.7%, 42.2% and 65.2% for the systems with the evacuated tube filled with aluminum foil, water and oil, respectively [25]. The maximum freshwater yield of the system was 0.78 $L/m^2 \cdot hr$ or 0.9333 $kg/m^2 \cdot hr$.

3. SODESAL SYSTEM DESIGN

This section explains the details of the SODESAL design including the theory and methodology for designing the system components. The SODESAL design was inspired by the experiment conducted at the Sharif University of Technology in Tehran, Iran which utilized a single parabolic solar trough mirror to concentrate sunlight onto an evacuated tube. The Sharif experimental design allowed the mirror to track and concentrate direct sunlight to analyze freshwater yields for desalination. The dimensions for the Sharif system's evacuated tube and parabolic mirror are listed below in Table 1 [25].

Table 1: Sharif System Specifications

Mirror Specification	Value/Type
Collector Aperture Area	$1.8m^2$
Collector Aperture	1 m
Receiver Diameter	47 mm
Receiver Length	1800 mm
Concentration Ratio	6.77
Parabola Height	176 mm
Rim Angle	79.31°
Focal Length	355 mm
Rim Radius	531 mm
Diameter of Receiver for Reflector with Perfect Shape and Alignment	4.95 mm
Allowable Misalignment for 100% Image Reflection	2.56°
Heat Transfer Fluid	Ethanol

An analysis of the Sharif's experimental design was conducted to understand how to develop a similar system utilizing a different sized evacuated tube, larger mirror and shorter focal length, while accommodating materials available in San Luis Obispo.

The system used in this SODESAL project consisted of four major components: an evacuated tube, a parabolic solar concentrator mirror, a tracking frame and a boiler. The evacuated tube converts absorbed sunlight into thermal energy by means of an internal heat transfer pipe and fluid. The parabolic solar concentrator mirror focuses sunlight to increase the solar energy into the evacuated tube. The tracking frame allows for adjustments of the mirror's surface based on the time of day and year. The boiler receives the thermal energy from the heat pipe and heats the internal water to produce steam for distillation.

3.1 Evacuated Tube

An evacuated tube, otherwise known as a "Sydney" tube or a "twin-tube" is a double layered glass-walled tube which converts sunlight into thermal heat (Figure 3.1). As sunlight travels through the outer glass layer of the evacuated tube, it passes through a vacuum and impacts a special absorbing layer on the surface of the inner glass tube. The air between the two layers of glass is evacuated to create this vacuum so that the air cannot cause convection losses between the surfaces during heat transfer.

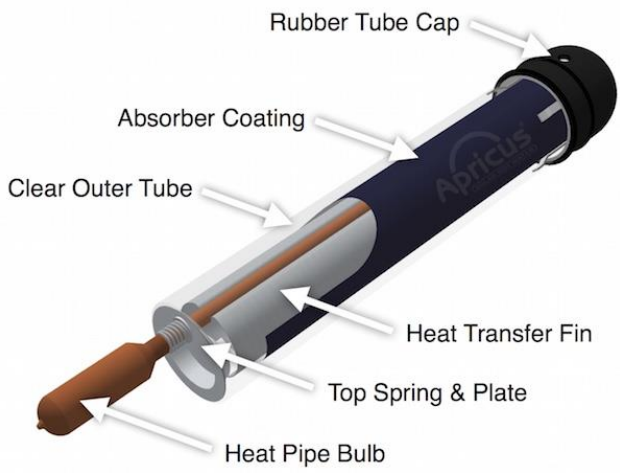

Figure 3.1: Apricus® Evacuated Tube [27]

The absorbed sunlight is converted to heat and is transferred to an aluminum heat transfer fin inside the inner glass tube. The aluminum fin and internal air heats up and transfers thermal energy to a copper pipe heat exchanger. The aluminum fin is shaped such that the copper tube is held directly in the middle of the tube and the outer face of the aluminum is touching the inner glass surface of the evacuated tube (Figure 3.2).

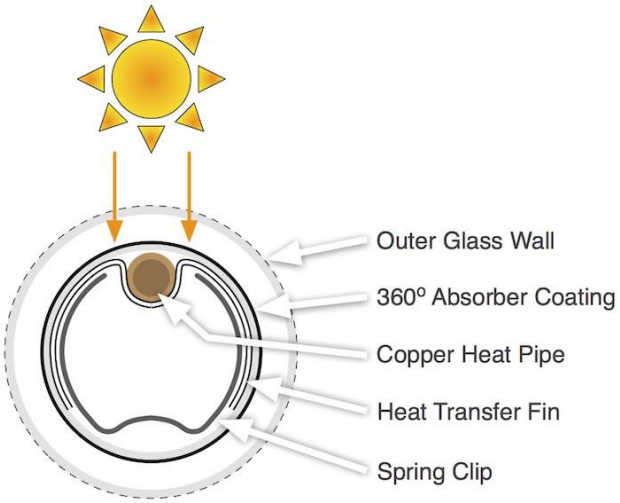

Figure 3.2: Apricus Evacuated Tube (open end) [27]

The copper pipe heat exchanger is filled with a water-glycol heat transfer fluid, which when heated, phase changes into a gas and travels up the length of the heat-pipe and condenses at the top. The gas cools and condenses in the bulb by transferring heat to a manifold and drips down the length of the copper heat pipe where it is heated once again by the evacuated tube and aluminum fin (Figure 3.3).

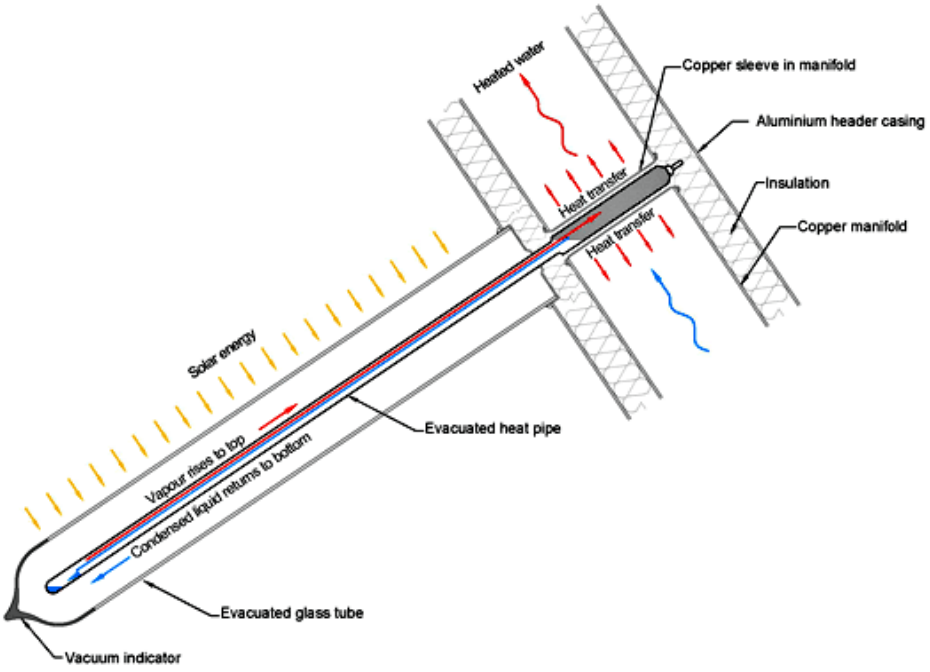

Figure 3.3: Condenser Heat Pipe Solar Thermal Collector [28]

A solar water heater uses sunlight to off-set or replace the energy required to heat water for a residential home or pool. Several evacuated tubes are placed side-by-side in a rack on either a roof or open sunlit area adjacent to the water source (Figure 3.4).

Figure 3.4: Solar Water Heater Collector System [29]

Evacuated tubes are readily available from solar water heater retailers ranging in lengths between 800-2100 mm, and their individual prices may make them economical for developing a small-scale solar desalination system. The evacuated tube used in the SODESAL experiment was supplied by Apricus®, a solar water heating company. The Apricus® evacuated tube had an approximate radius of 29 mm, operating length of 1.8 m and a glass wall thickness of 1.8 mm (Figure 3.5) [30].

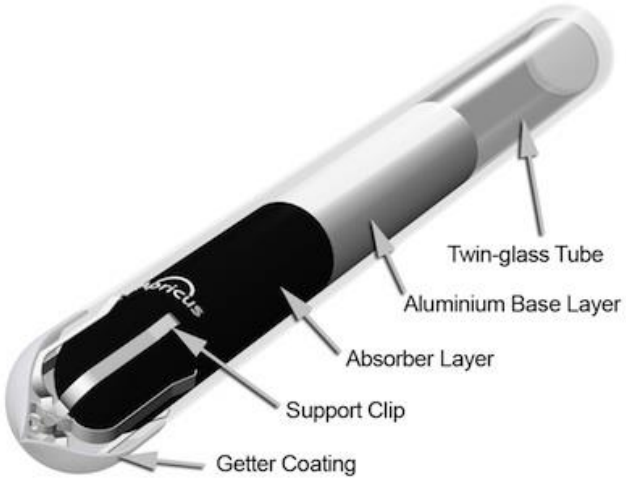

Figure 3.5: Apricus® Evacuated Tube Used in SODESAL Experiment [30]

The evacuated tube is made of a borosilicate glass material similar to Pyrex which provides strength against impacts like hail and maintains a light transparency of > 92% through a 2mm wall thickness [30]. A barium getter is installed inside the evacuated chamber which helps soak up gases that may enter the vacuum chamber and compromise the tube. The internal absorber coating consists of an aluminum layer on the outside of the inner glass tube followed by a layer of a dark colored aluminum nitride material. A single tube can provide over 60 Watts or 204 BTU of water heating output when under strong sunlight [30].

The evacuated tube used in this SODESAL system was selected from a solar water heating system since it had the same length and similar characteristics as the Sharif evacuated tube. The evacuated tube is open on one end to allow the copper heat-pipe to insert into the solar water heater's manifold. The evacuated tube must be angled to allow for the internal heat transfer fluid to recirculate in the copper heat-pipe. Evacuated tubes used in large-scale CSP systems are typically open on both ends to allow the heat transfer fluid to travel horizontally through the evacuated tube and along the focal point of the PTSC mirror. Running evacuated tubes horizontally allows for multiple tubes to collectively heat a heat transfer fluid in an array system (Figure 3.6).

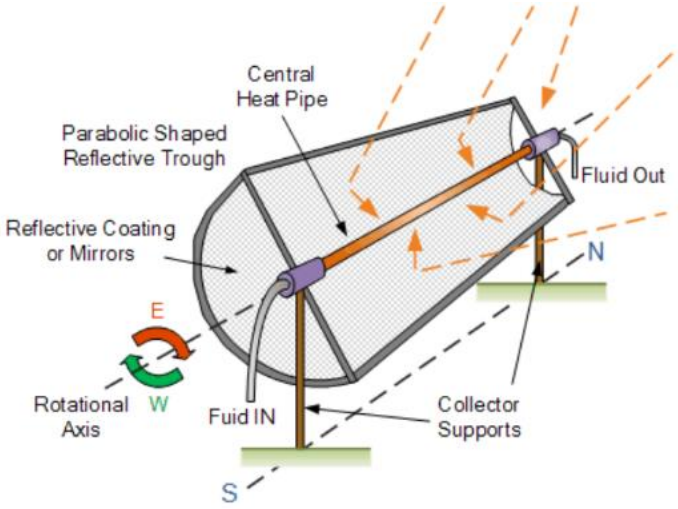

Figure 3.6: Parabolic Trough Solar Concentrator Mirror with Horizontal Evacuated Tube [31]

3.2 Parabolic Trough Solar Concentrator Mirror

Parabolic trough solar concentrator mirrors are typically used for large commercial scale systems for both power generation and water treatment in addition to small-scale systems for residential hot water (Figures 3.7 & 3.8).

Figure 3.7: Residential CSP Water Heater [32]

Figure 3.8: Large Scale CSP Plant [33]

Both large and small-scale systems demonstrate the scalability of parabolic solar concentrators and their use for heating up water for different sized demands. The mirrors in these systems are

troughs since their design reflects sunlight at a point across the length of the mirror. The evacuated tube runs along the focus point of the mirror and serves as the “target” toward which sunlight is concentrated. Targeting the evacuated tube requires determining the size, shape and location of the suns reflected image onto the concentrated surface. Analyzing the parabolic mirror’s geometric properties determines the theoretical reflected sunlight concentration onto the evacuated tube or receiver.

The geometric properties for a parabolic solar concentrator mirror include the aperture area, rim angle, rim radius, parabola height and focal length (Figures 3.9 & 3.10). These properties determine the parabolic mirror’s concentration ratio, the required diameter of a cylindrical receiver for a reflector with ideal shape and alignment, and the parabolic mirror’s maximum allowable misalignment before 100% of the sun’s image is no longer reflected [3].

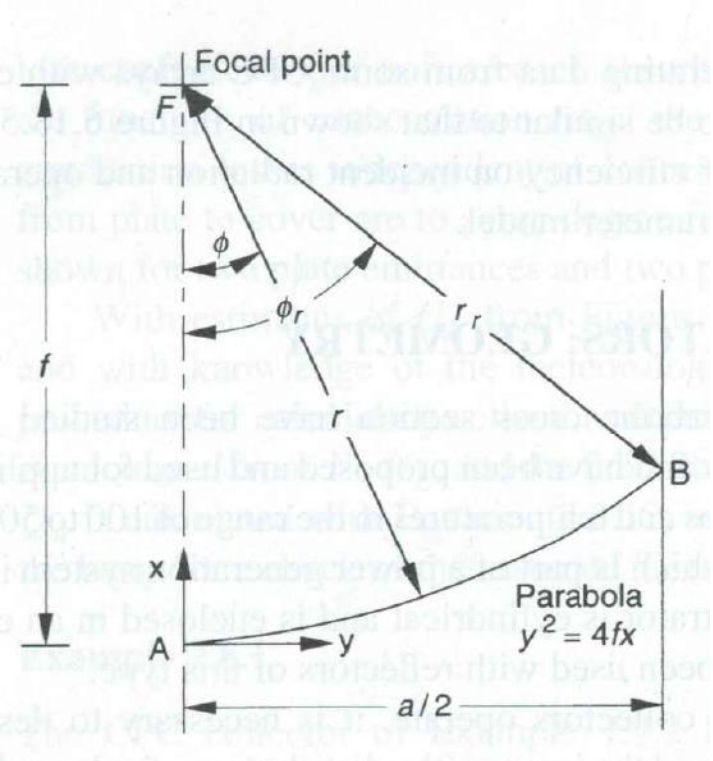

Figure 3.9: Geometric Properties of Mirror [3]

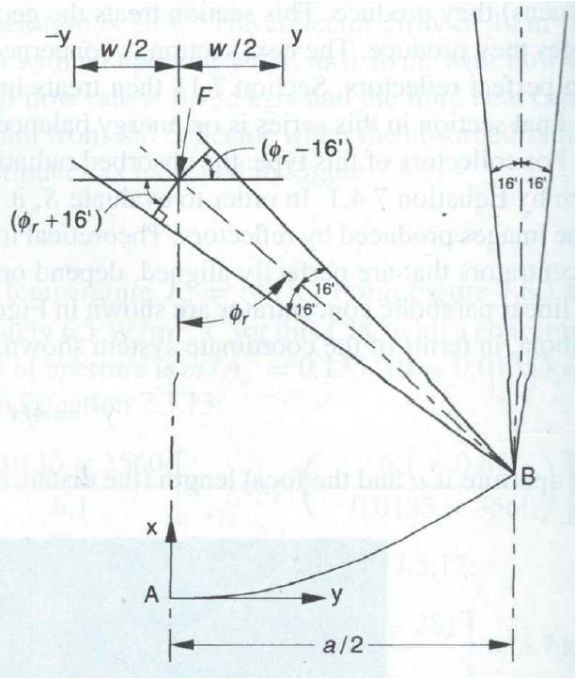

Figure 3.10: Geometric Properties of Reflected Image [3]

Aperture is the width of area or “window” of sunlight that enters the parabolic mirror. The aperture of a parabolic mirror determines the total input of sunlight radiation into the system before concentration. The rim angle represents the angle between the outer edge of the parabolic mirror to the focal point or receiver, which is located at half the distance of the mirror’s aperture and above the parabola’s vertex. The rim radius is the distance between the focal point and the outer edge of the parabolic mirror. The parabola height is the height of the edge of the mirror located half the aperture from the vertex. The focal length is the distance between the mirror’s focal point and vertex. Equations 1 – 4 were used to calculate the properties to design the parabolic mirror where (f) is the focal length and (a) the aperture width[3].

Equation 1: Aperture Area $A_a = (Tube\ Length)\ X\ (Aperture\ Width)$ [3]

Equation 2: Rim Angle $\Phi_r = tan^{-1}\left[\frac{8(f/a)}{16(f/a)^2-1}\right] = sin^{-1}\left(\frac{a}{2r_r}\right)$ [3]

Equation 3: Rim Radius $r_r = \frac{2f}{1+\cos\Phi}$ [3]

Equation 4: Parabola Height $h = \frac{a^2}{16f}$ [3]

The concentration ratio of a parabolic solar concentrator is the ratio between the aperture area and the receiver's total surface area. The concentration ratio is used to compare parabolic solar concentrator systems and the overall capability to concentrate sunlight. Higher concentration ratios can mean the parabolic mirror has a relatively large surface area or that the receiver is relatively small. Larger parabolic mirrors can increase the capital costs of a system whereas a smaller receiver can increase the difficulty for accurate sunlight tracking since the target for concentrating sunlight onto is small. The maximum concentration ratio for a linear concentrator is 212. However, if the mirror is circular and utilizes dual-axis tracking, the maximum possible concentration ratio becomes 45,000 [3]. Higher concentration ratios require more precise optics of both the mirror and tracking system and will yield in a higher temperature of the delivered energy to the system [3].

The required diameter for a cylindrical receiver for a reflector with ideal shape and alignment is calculated using Equation 5 to determine the theoretical receiver size for the given parabolic mirror properties [3].

Equation 5: Diameter of Cylindrical Receiver $D = 2r_r \sin 0.267 = \frac{a \sin 0.267}{\sin\Phi_r}$ [3]

If the diameter for the theoretical receiver size is less than the actual receiver diameter then the parabolic mirror's concentration of sunlight will work assuming its shape and alignment is ideal (Figure 3.11) [3].

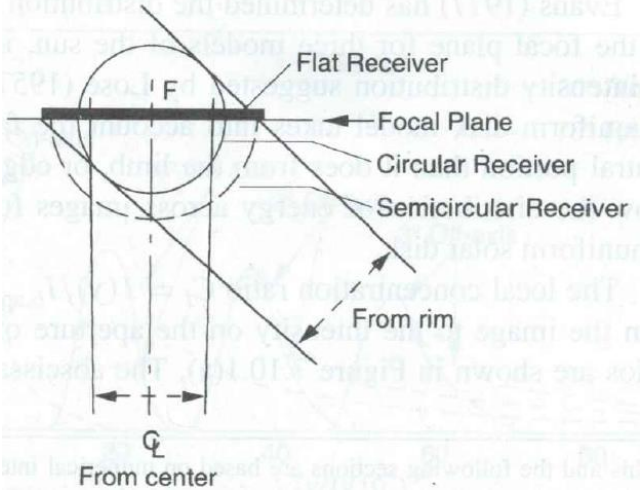

Figure 3.11: Reflected Radiation from Rim onto Receiver [3]

The maximum allowable misalignment before 100% of the sun's image is no longer reflected represents a designed allowable error within the parabolic mirror's sunlight concentration. Accurate sunlight tracking is critical for the performance of a parabolic solar concentrator mirror since the mirror utilizes direct sunlight normal to the mirror's surface to achieve concentration. The shape of the parabolic mirror for the SODESAL system was designed using the Parabolic Trough Solar Concentrator - Wolfram CDF Player software [34]. The program allows for several adjustable design parameters including, tube radius, half aperture width, focal length and the degrees of misalignment. The selected dimensions for the SODESAL system were determined after analyzing the mirror dimensions for the Sharif design (Figure 3.12) [25].

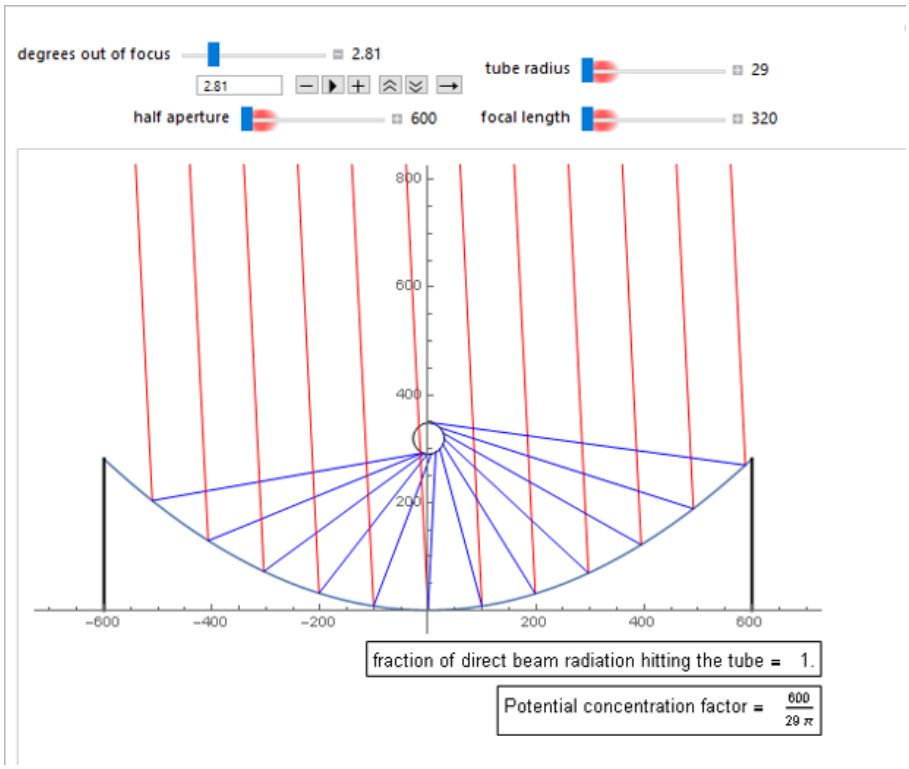

Figure 3.12: Wolfram Parabolic Trough Solar Concentrator Designer [34]

The focal length of the mirror was determined after iterating different focal lengths until the optimal allowable misalignment to continue yielding a full image reflection on the concentrated surface was found given an aperture width of 1200mm. The SODEAL mirror design allows for 2.81 degrees of misalignment before any reduction in reflected image.

The final parabolic specifications for the SODESAL mirror are shown in Table 2, compared to the dimensions for the Sharif study. The differences in mirror dimensions between the Sharif and SODESAL designs is due to the differences in evacuated tube diameters and the effect on concentration ratio. Since the SODESAL evacuated tube was larger it required a greater mirror surface area to achieve a similar concentration ratio as Sharif's. Maximizing the degrees of

allowable misalignment altered the SODESAL mirror dimensions to also have a larger parabola height and shorter focal length.

Table 2: Sharif and SODESAL Parabolic Mirror Specifications

Mirror Properties	Sharif	SODESAL
Collector Aperture Area	1.8m^2	2.16 m^2
Collector Aperture	1 m	1.2 m
Receiver Diameter	47 mm	58 mm
Receiver Length	1800 mm	1800 mm
Concentration Ratio	6.77	6.5857
Parabola Height	176 mm	281 mm
Rim Angle	79.31˚	86.30˚
Focal Length	355 mm	320 mm
Rim Radius	531 mm	601 mm
Diameter of Receiver for Reflector with Perfect Shape and Alignment	4.95 mm	5.60 mm
Allowable Misalignment for 100% Image Reflection	2.56˚	2.81˚
Heat Transfer Fluid	Ethanol	Water-glycol mixture

Equation 6 represents the parabolic shape required for the mirror to concentrate sunlight where f is the focal length from the base of the mirror to the vertex, x is the distance away from the base of the mirror and y is the correlating height of the mirror's surface given x. The parabolic equation for the SODESAL system is shown in Equation 7.

Equation 6: Parabolic Shape $$y = \frac{x^2}{4f}$$ [3]

Equation 7: SODESAL Parabolic Shape $$y = \frac{x^2}{4(320mm)} = 0.0007813x^2$$ [3]

The parabolic shape for the mirror was plotted on Microsoft Excel with an aperture width of 1.2 meters (Figure 3.13).

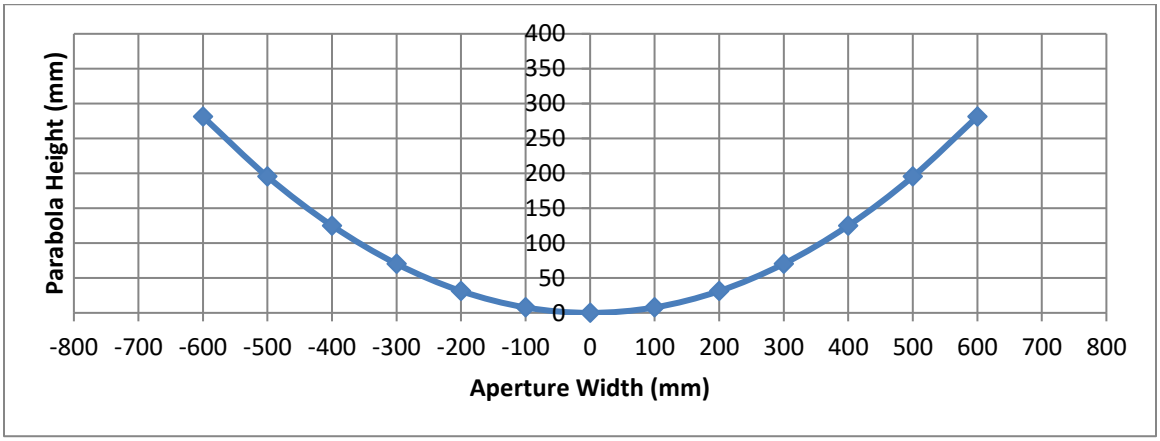

Figure 3.13: SODESAL Parabolic Curve

The arc length for the parabolic mirror was calculated using Equation 8, where $\boldsymbol{a}$ and $\boldsymbol{b}$ represent the half aperture widths in both x directions and $\frac{\boldsymbol{dy}}{\boldsymbol{dx}}$ is derived from Equation 6. The calculated arc length for the SODESAL system was 1357.88mm by integrating Equation 9 [3].

Equation 8: Parabolic Surface Length $L = \int_a^b \sqrt{1 + \left(\frac{dy}{dx}\right)^2}\, dx$ [3]

Equation 9: SODESAL Parabolic Surface Arc Length $L = \int_{-600}^{600} \sqrt{1 + (0.0015625x)^2 dx}$ [3]

3.3 PTSC Mirror Construction

The SODESAL parabolic surface equation was used to plot the X-Y coordinates of the parabolic shape into a laser cutting program using Equation 7 (Figure 3.14). Laser cutting was used to maximize the accuracy and shape of the parabolic surface.

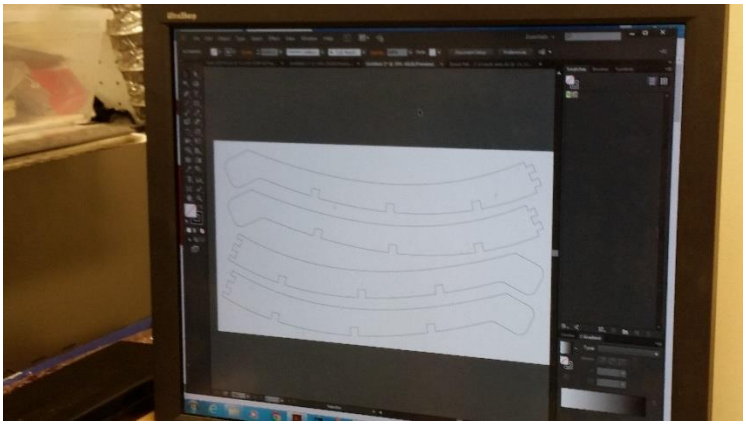

Figure 3.14: Laser Cutting Program

The laser cutter etched out the desired parabolic shape onto wood panels used to create the ribs for the parabolic mirror (Figures 3.15). Only half a rib could fit within the laser cutter aperture; the ribs were designed to be joined in the middle with a jigsaw pattern (Figure 3.16).

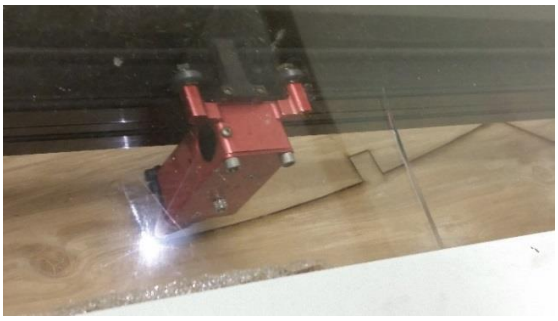

Figure 3.15: Laser Cutter

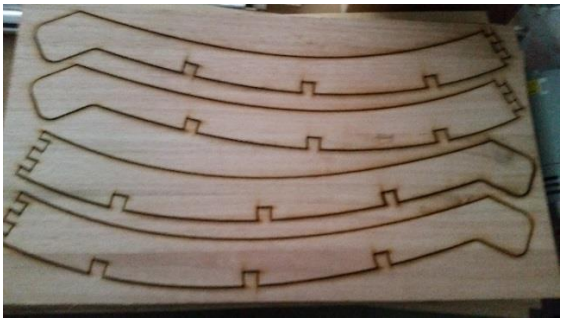

Figure 3.16: Finished Laser Cut Ribs

Wood was selected as the rib material due to its low cost, low weight and ease in manufacturing. The width of a single wood panel was too thin to support the weight of the mirror, so each complete rib contains three sections that were glued and clamped together for at least 24 hours (Figure 3.17).

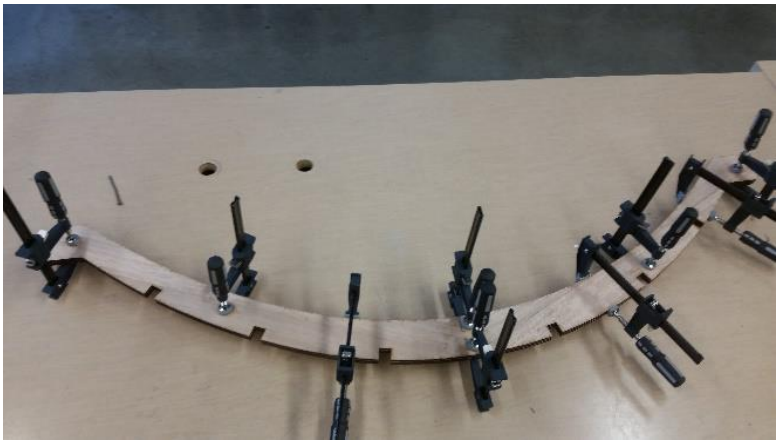

Figure 3.17: Rib Assembly

The parabolic surface of the ribs was sanded to smooth out any uneven edges between the adjacent pieces without compromising the parabolic shape. The ribs also had notches cut out of the bottom edge to allow for a rod to connect the ribs together (Figure 3.18).

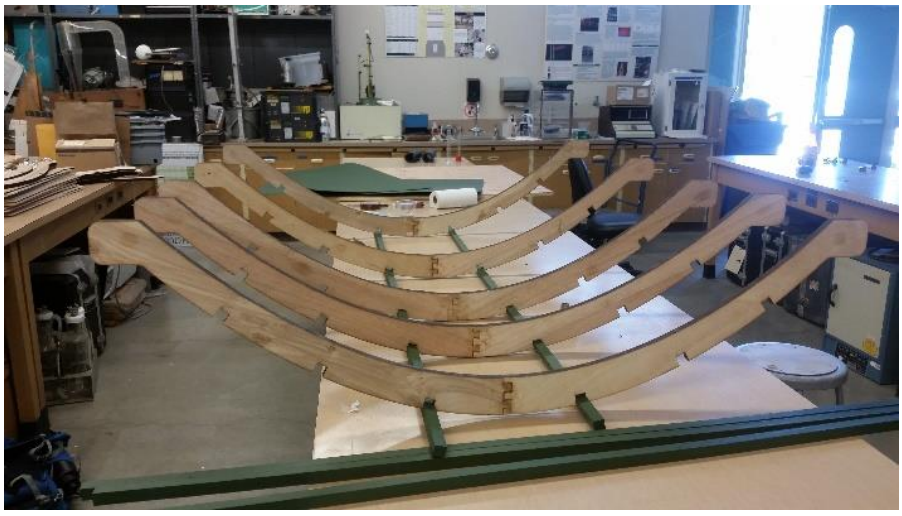

Figure 3.18: Mirror Rib Skeleton

The rods connecting the ribs were glued and hammered into place. Each joint was clamped and allowed to cure for 1 day after applying a wood glue (Figure 3.19).

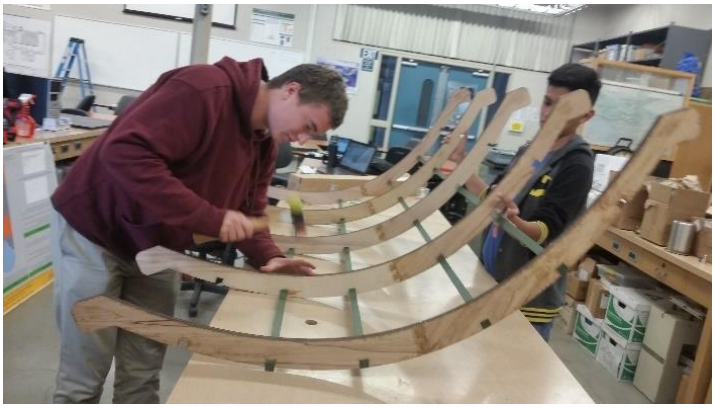

Figure 3.19: Mirror Rib Assembly with Support Rods

Two endcaps were cut out of a thick piece of plywood to hold the ribs and cross beams together with enough height to support the evacuated tube (Figures 3.20 & 3.21).

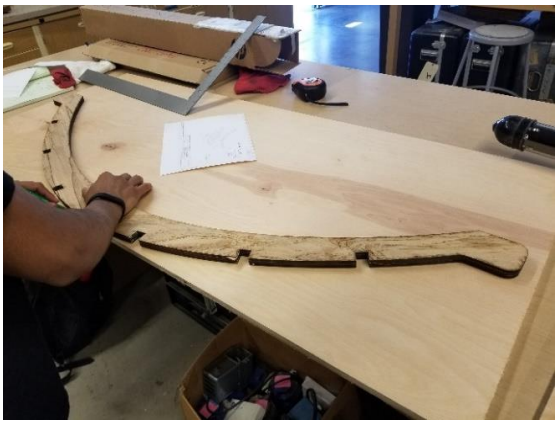

Figure 3.20: End Cap Design

Figure 3.21: End Cap Assembly

A thin sheet of wood utility paneling was selected from a local hardware store for the base of the parabolic mirror due to its flexibility and low material cost. The utility panel was secured with finishing screws and sanded until smooth (Figure 3.22).

Figure 3.22: Parabolic Mirror with Wood Utility Panel

Each side of the parabolic mirror required an endcap to hold the ribs and supports together. A section of the endcap was removed to allow the evacuated tube to fit. The SODESAL system required the parabolic mirror to rotate around the axis of the evacuated tube so lead screws were attached to each endcap to allow for adjustments in focal length (Figure 3.23). The lead screws attach to a turntable bearing which is mounted on the inside face of the wooden tracking frame (Figure 3.24).

Figure 3.23: End Cap with Lead Screw Figure 3.24: Turntable Bearing

3.4 Reflective Material

The material used for the reflective surface was ReflecTech® mirror film. ReflecTech® mirror film is used for commercial parabolic trough concentrating solar power systems. The mirror film is a silver polymer film developed at the National Renewable Energy Laboratory (NREL) where research focused on cost reduction and increasing the durability of parabolic trough collectors. SkyFuel® currently owns the exclusive license to manufacture ReflecTech® and the company states that their product can withstand the equivalent of 35 years of outdoor UV dosage with no degradation and no loss in reflectance. The material also maintains a resistance to delamination after a water immersion test for 60 days [35]. The ReflecTech® material ships in a 4ft wide roll and costs around $\$31.00/m^2$ (Figure 3.25).

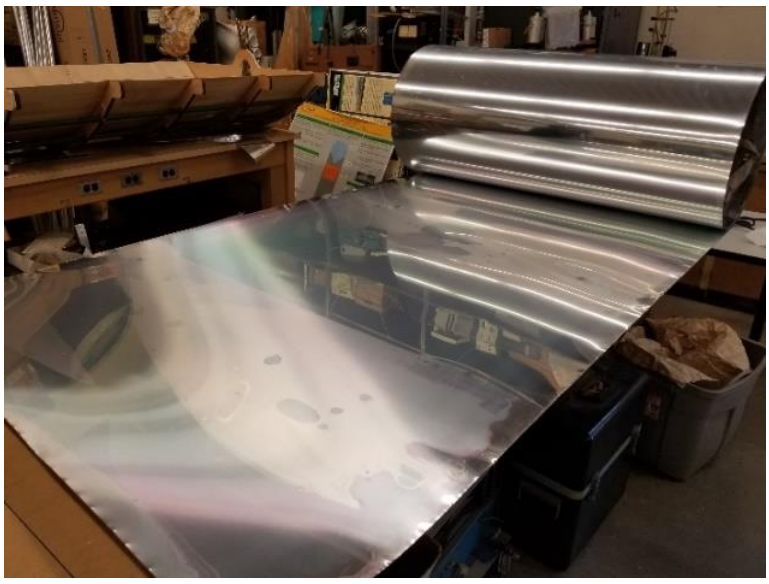

Figure 3.25: ReflecTech® Mirror Film

Two sections of ReflecTech® were used to cover the parabolic surface required for the parabolic mirror. The reflective material was pulled across the top of utility panel and cut so that the entire arc length was covered. The width of the second piece was cut to fit the length of the

parabolic mirror and each section was screwed into the wood utility panel with finishing screws. The two pieces have slightly different parabolic surfaces and the difference in reflection between the two pieces can be seen in Figure 3.26.

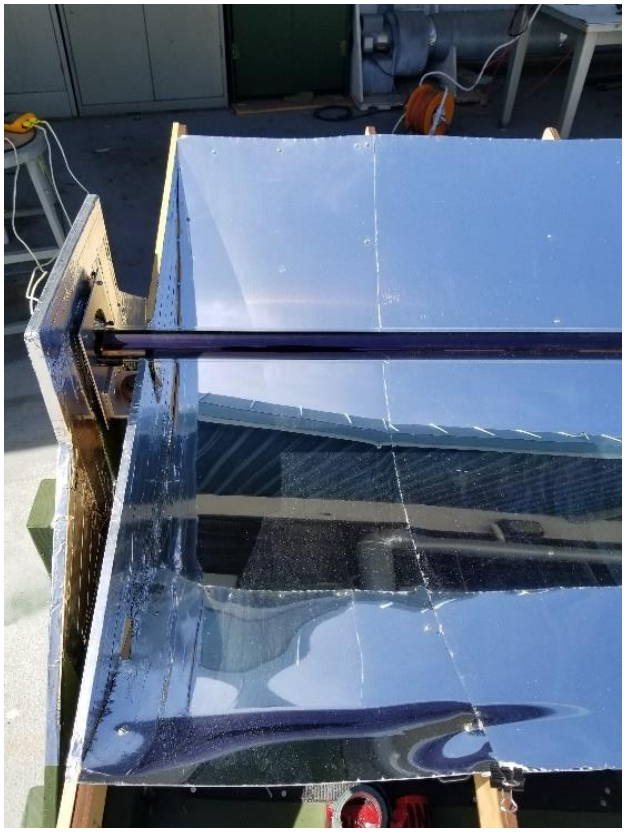

Figure 3.26: Joining of ReflecTech ® Surfaces with Finishing Screws

The material has a specular reflectance of 94% and contains a peel-off release liner that covers the material until application, making it an idea choice for installing onto an experimental surface (Figures 3.27 & 3.28) [35].

Figure 3.27: Removal of ReflecTech® Protective Liner

Figure 3.28: ReflecTech® Final Application

3.5 Tracking Frame

Accurate tracking and adjustments of the parabolic solar concentrator mirror are necessary to concentrate direct sunlight onto the evacuated tube for operation. Since the evacuated tube used in the SODESAL system was originally designed for a solar water heater, a minimum angle is required to allow the internal heat transfer fluid to circulate. The frame for the SODESAL system needed to support the weight of the evacuated tube, mirror and boiler while also allowing for the adjustment of the mirror's focal length, rotation, and slope throughout the year. The frame of the SODESAL system was constructed out of wood to reduce construction costs and ease the fabrication process of the system (Figure 3.29).

Figure 3.29: SODESAL Frame (Elevated)

Figure 3.30: SODESAL Frame (Collapsed)

The frame was designed to carry up to 100 pounds during operation. High winds could tip the system when the mirror is rotated so the base of the frame was designed to be wide enough to prevent tipping and increase the system mass. Lockable caster wheels were attached to the bottom of the frame to allow for easy maneuvering of the system for alignment (Figure 3.30).

An adjustable boiler holder was designed to allow for different boiler sizes if the boiler volume was changed by implementing a V-shaped holder while also allowing for the entire holder to adjust up and down by moving securing bolts through channels on the endcap. The bottom face of the boiler rests next to the outer face of the endcap so that the evacuated tube's copper heat-pipe can insert for heat transfer (Figures 3.31 & 3.32).

Figure 3.31: Boiler Holder

Figure 3.32: Boiler Holder Adjustment

The weight of the evacuated tube rests on the bottom endcap when elevated, however the evacuated tube cannot rotate due to the heat pipe and how the boiler is secured. A gear system was designed to allow for the mirror to rotate around the evacuated tube. A gear box was constructed around the gear to protect operators and the motor-chains system from environmental damage (Figures 3.33 - 3.35).

Figure 3.33: Tracking Gear

Figure 3.34: Bottom Endcap Gearbox and Evacuated Tube Holder

The SODESAL system was designed to also operate at a horizontal configuration if necessary (Figure 3.36). For horizontal operation a solar water heater pipe must be replaced with a pumped heat transfer fluid system that will loop inside the evacuated tube.

Figure 3.35: SODESAL System (Elevated)

Figure 3.36: SODESAL System (Horizontal) with no Gear Box

3.6 Tracking Frame Alignment

Alignment is critical for a solar collector to capture the most sunlight possible for concentration. The sunlight tracking methods used in the experiments required the parabolic mirror to be aligned along either the polar E-W or N-S axis (Figures 3.37 & 3.38).

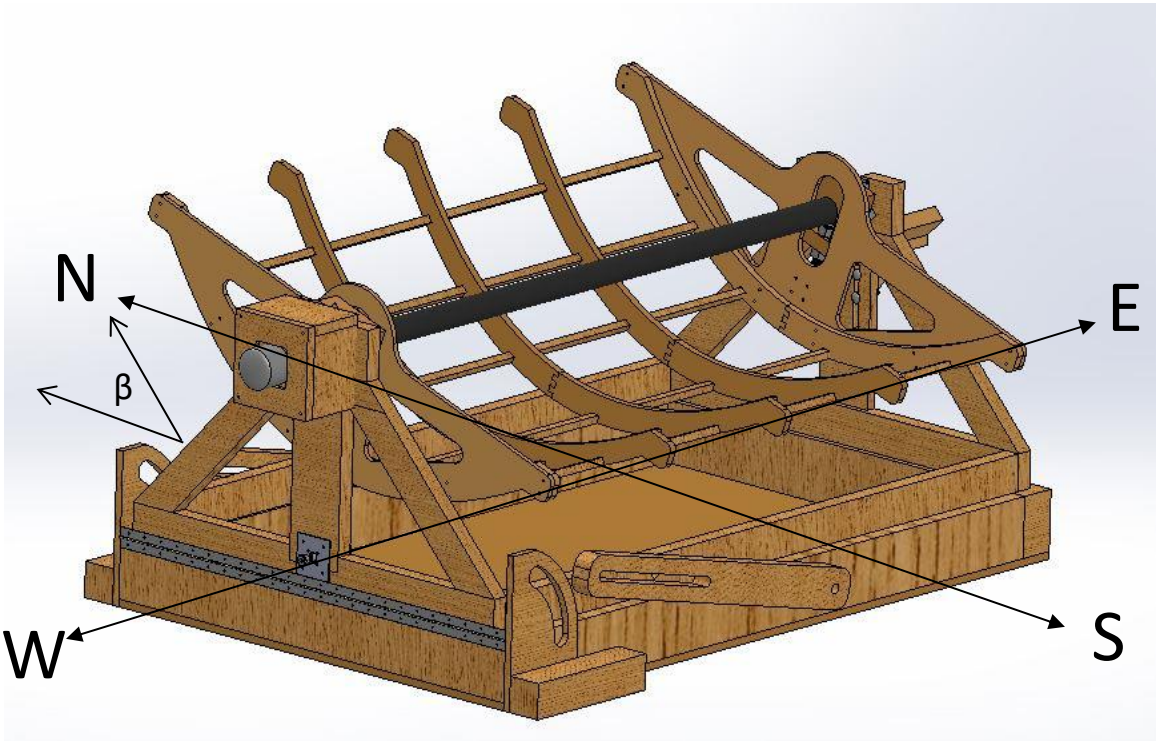

Figure 3.37: E-W Alignment, (prepared by Teyvon Brooks)

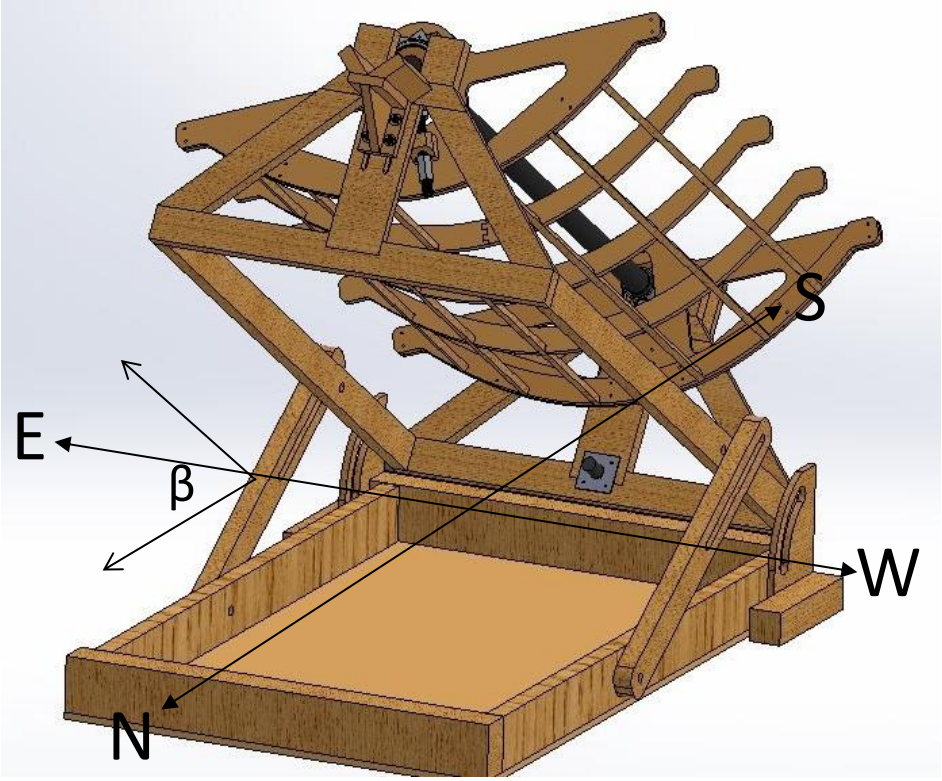

Figure 3.38: N-S Alignment, (prepared by Teyvon Brooks)

An ancient method for finding true north, the shadow-stick method, was used to find true north. A stick was place upright normal to the ground surface and the location of the edge of the stick's shadow was marked every 15 minutes. The line of marks indicates the direction of the earth's E-W axis and was used to align the parabolic mirror (Figure 3.39).

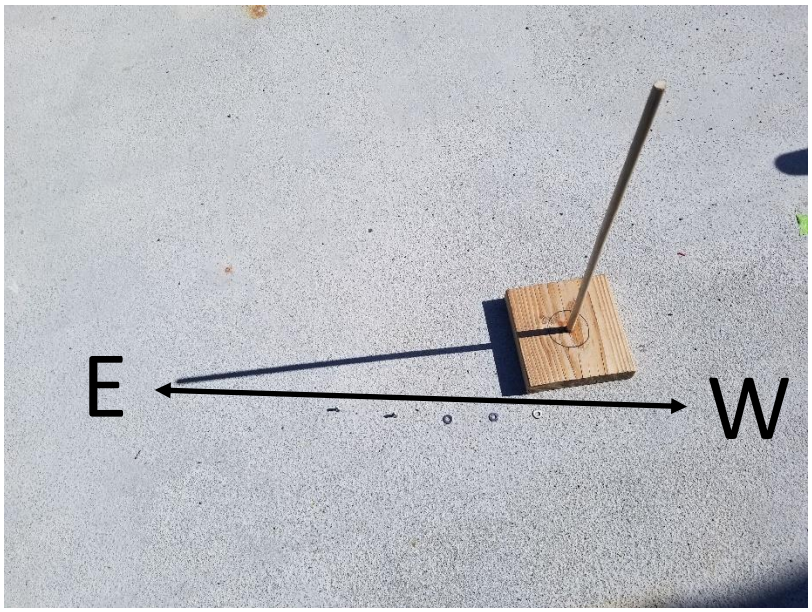

Figure 3.39: Shadow-Stick Method for E-W Axis Alignment

3.6.1 Sun Tracking Angles

The angles that determine the position of the sun's beam radiation for a solar tracking system is the location's latitude (Ø), declination and sun hour angle.

The latitude is the angular location north or south of the equator, north positive; - $90^o \leq Ø \leq 90^o$. The latitude (Ø) for the SODESAL system was determined using an online Global Positioning System (GPS) and is 35.3013° N [37].

The declination (δ) is the angular distance of a point north or south of the celestial equator and changes daily. The declination and is calculated using Equation 10 which requires the latitude of the system's location and the day (n) of the year.

Equation 10: Declination $$\delta = 23.45 \sin\left(365 \frac{284+n}{365}\right)$$ [16]

The declination is used to determine the angle of incidence (θ), which is the angle between the solar beam radiation on a surface and the normal of that surface (Figure 3.40)

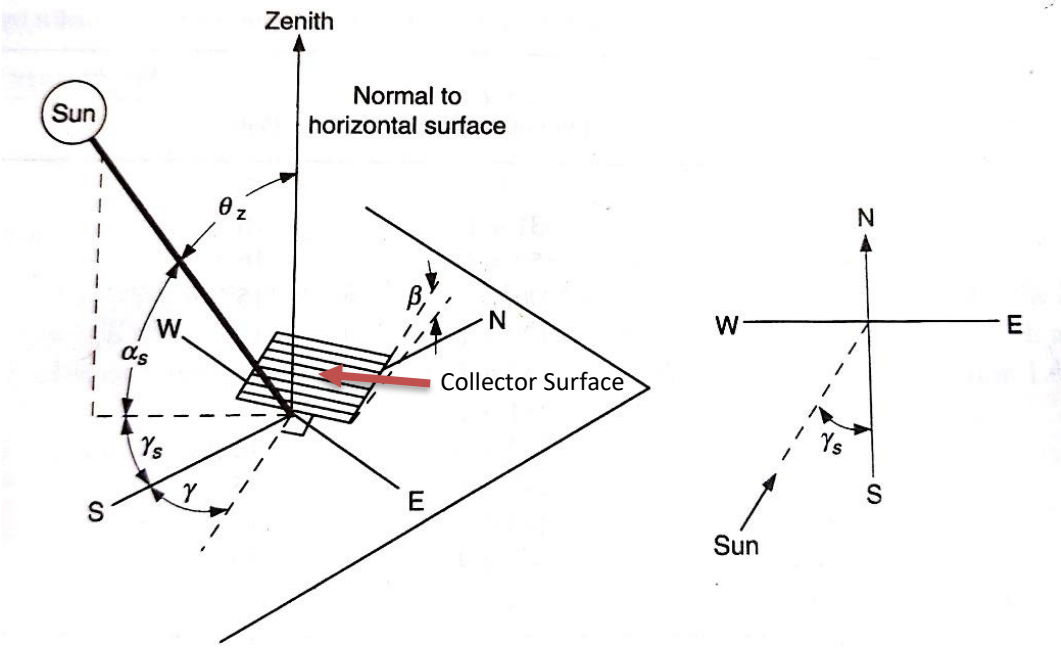

Figure 3.40: Zenith angle ($\boldsymbol{\theta_z}$), slope ($\boldsymbol{\beta}$), surface azimuth angle ($\boldsymbol{\gamma}$), solar azimuth angle ($\boldsymbol{\gamma_s}$), solar altitude angle ($\boldsymbol{\alpha_s}$) for a tilted surface [3]

Sun Hour Angle (ω) is the angular displacement of the sun east or west of the local meridian due to the rotation of the earth on its axis at 15° per hour; morning negative, afternoon positive. The sun hour angle is used for calculating the sun's position in respect to solar time and is used for continuous tracking. The sun hour angle (ω) is 0° at solar noon. For example, if solar noon occurs at 1:00 pm, the sun hour angle at 2 pm would be 15° since only one hour has elapsed from when the sun traveled west of the local meridian.

3.6.2 Solar Noon

Solar noon occurs when the sun crosses the local meridian and reaches its highest position in the sky. The exact time for solar noon fluctuates every day for each location on the earth. Solar noon was found using the NOAA Solar calculator for each test day. The calculator receives the latitude, longitude, and time zone to calculate the time for solar noon [36]. The NOAA solar calculator for one of the days of data collection is in Figure (3.41).

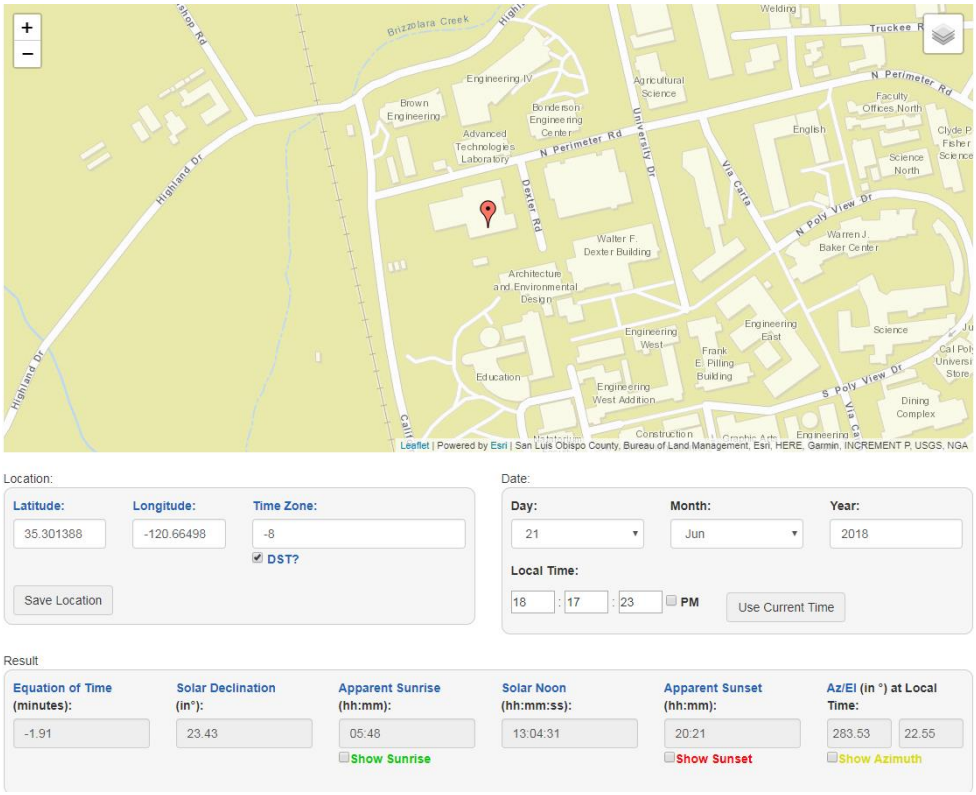

Figure 3.41: NOAA Solar Calculator – Cal Poly Test Location - June 21st, 2018 [37]

The shadow cast by the tracking frame at solar noon is another way to verify that the mirror is aligned along the E-W axis (Figure 3.42).

Figure 3.42: Solar Noon Shadow, arrows indicate rib shadow

3.7 Sun Tracking Methods

There are six methods for which a surface can track the sun, depending on whether the mirror is aligned parallel to the earth's true north-south or east-west axis, as well as the axis around which the mirror is rotated.

3.7.1 Method 1 Tracking

The simplest method for tracking the sun is when the horizontal mirror surface is aligned along the east-west axis. Only a single daily adjustment is required so that the beam radiation is normal to the mirror at solar noon each day. The slope and angle of incidence for Method 1 tracking is calculated using Equations 11 and 12.

Equation 11: Method 1 Slope $$\beta_{M1} = |\emptyset - \delta|$$ [3]

Equation 12: Method 1 Angle of Incidence $\cos\theta = \sin^2\delta + \cos^2\delta\cos\omega$ [3]

The surface azimuth angle for Method 1 tracking will be 0° or 180° depending on the latitude and declination and is found using Equation 13.

Equation 13: Method 1 Surface Azimuth Angle $\gamma = \begin{cases} 0° & if\ \emptyset - \delta > 0 \\ 180° & if\ \emptyset - \delta \leq 0 \end{cases}$ [3]

3.7.2 Method 2 Tracking

Method 2 tracking is a plane that is rotated about a horizontal east-west axis with continuous mirror slope (β) adjustment toward the sun. Method 2 tracking improves the alignment of the mirror by minimizing the angle of incidence of the sun's beam radiation onto the mirror's surface. A motor drives a chain and gear system to turn the mirror to the ideal slope depending on the desired moment's sun hour angle. The slope and angle of incidence for Method 2 tracking is calculated using Equations 14 and 15.

Equation 14: Method 2 Slope $\tan\beta = \tan\theta_z|\cos\gamma_s|$ [3]

Equation 15: Method 2 Angle of Incidence $\cos\theta = (1 - \cos^2\delta\sin^2\omega)^{1/2}$ [3]

The surface azimuth angle for Method 2 tracking will change between 0° and 180° if the solar azimuth angle passes through $\pm$90° and is found in either hemisphere using Equation 16.

Equation 16: Method 2 Surface Azimuth Angle $\gamma = \begin{cases} 0° & if\ |\gamma_s| < 90 \\ 180° & if\ |\gamma_s| \geq 90 \end{cases}$ [3]

Method 2 continuous tracking is performed using an electric motor that is coupled with an Arduino solar cell tracker. The Arduino tracker is programed with the values to rotate the mirror to the required slope for a given sun hour angle.

3.7.3 Method 3 Tracking

Method 3 tracking is a plane rotated about a horizontal north-south axis with continuous adjustment. Like Method 2, this type of tracking will minimize the angle of incidence and is used when E-W axis orientation is not ideal for the system's area. The slope and angle of incidence for Method 3 tracking is calculated using Equations 17 and 18.

Equation 17: Method 3 Slope $$\tan\beta = \tan\theta_z|\cos(\gamma - \gamma_s)|$$ [3]

Equation 18: Method 3 Angle of Incidence $$\cos\theta = (\cos^2\theta_z + \cos^2\delta\sin^2\omega)^{1/2}$$ [3]

The surface azimuth angle for Method 3 tracking will be 90° or -90° depending on the sign of the solar azimuth angle and is find using Equation 19.

Equation 19: Method 3 Surface Azimuth Angle $$\gamma = \begin{cases} 90° & if\ \gamma_s > 0 \\ -90° & if\ \gamma_s \leq 0 \end{cases}$$ [3]

3.7.4 Method 4 Tracking

Method 4 tracking is a plane with a fixed slope rotated about a vertical axis. Method 4 tracking is used for systems with a fixed slope. Some small-systems have an evacuated tube filled with a fluid medium to increase thermal efficiency so a system with a fixed slope is idea so that the contents of the evacuated tube do not still during operation.

The angle of incidence is minimized when the surface azimuth and solar azimuth angles are equal. The slope and angle of incidence for Method 4 tracking is calculated using Equations 19 and 20.

Equation 19: Method 4 Slope $$\beta = constant$$ [3]

Equation 20: Method 4 Angle of Incidence $$\cos\theta = \cos\theta_z\cos\beta + \sin\theta_z\sin\beta$$ [3]

The surface azimuth angle for Method 4 is equivalent to the solar azimuth angle since the tracker rotates about a vertical axis, Equation 21.

Equation 21: Surface Azimuth Angle $$\boldsymbol{\gamma = \gamma_s}$$ [3]

3.7.5 Method 5 Tracking

Method 5 tracking utilizes a plane rotated about a north-south parallel to the earth's axis with continuous adjustment. Method 5 tracking is used when the surface azimuth angle does not track the solar azimuth angle and a non-horizontal north-south axis. The slope and angle of incidence for Method 5 tracking is calculated using Equations 22 and 23.

Equation 22: Method 5 Slope $$\tan\beta = \frac{\tan\emptyset}{\cos\gamma}$$ [3]

Equation 23: Method 5 Angle of Incidence $$\cos\theta = \cos\delta$$ [3]

The surface azimuth angle for Method 5 is calculated using Equation 24 and requires additional calculation of two constants, C_1 and C_2.

Equation 24: Method 5 Surface Azimuth Angle $$y = \tan^{-1}\frac{\sin\theta_z \sin\gamma_s}{\cos\theta' \sin\emptyset} + 180C_1C_2$$ [3]

Where $$\cos\theta' = \cos\theta_z \cos\emptyset + \sin\theta_z \sin\emptyset \cos\gamma_s$$

$$C_1 = \begin{cases} 0 & if \left(\tan^{-1}\frac{\sin\theta_z \sin\gamma_s}{\cos\theta' \sin\emptyset}\right)\gamma_s \geq 0 \\ +1 & otherwise \end{cases}$$

$$C_2 = \begin{cases} +1 & if\ \gamma_s \geq 0 \\ -1 & if\ \gamma_s < 0 \end{cases}$$

3.7.6 Method 6 Tracking

Method 6 tracking is used when a plane is continuously tracked about two axes. Method 6 tracking is typically used for parabolic dish systems and maximizes solar radiation into the collector since the incident angle is minimized in both axes. The slope for Method 6 tracking is equal to the zenith angle, Equation 25 and the angle of incidence is found using Equation 26. The surface azimuth angle is equal to the solar azimuth angle, Equation 27.

Equation 25: Method 6 Slope $\beta = \theta_z$ [3]

Equation 26: Method 6 Angle of Incidence $\cos\theta = 1$ [3]

Equation 27: Method 6 Surface Azimuth Angle $\gamma = \gamma_s$ [16]

The SODESAL system's design can use Methods 1-5 for solar tracking. Method 6 would require an actuator strong enough to support the weight of the raised frame and would need to continuously adjust the slope of the mirror. The tracker's capabilities are demonstrated in Figures (3.43 – 3.45). Method 4 was utilized for Phase 1 of the experiment and Method 1 for Phase 2. Method 4 tracking provided the closest method of tracking to the Sharif study due to the necessary operating angle of the PTSC to allow the copper heat-pipe transfer fluid to circulate. Method 1 tracking was used for Phase 2 due to its simplicity for operation.

Figure 3.43: Partially raised SODESAL tracking

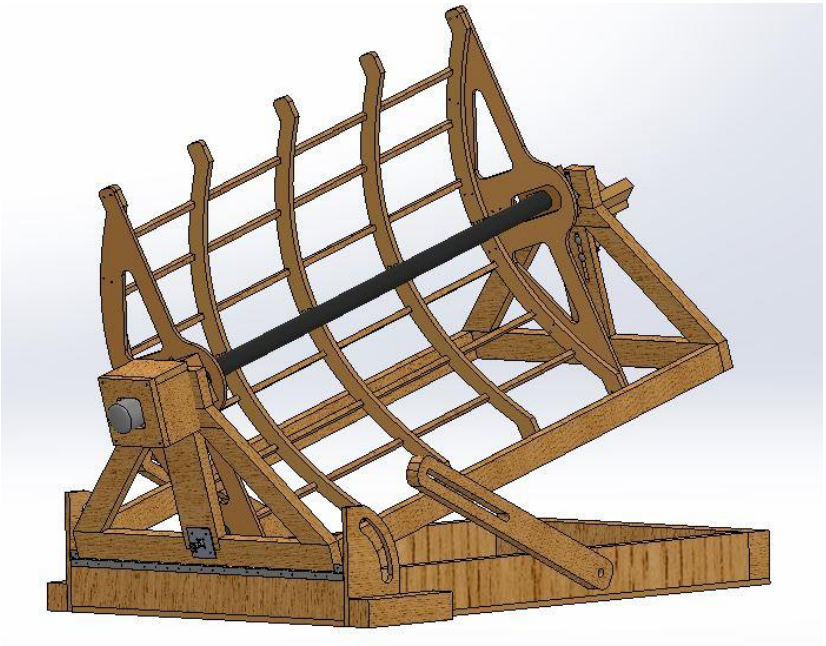

Figure 3.44: Partially raised SODESAL tracking with full rotation

Figure 3.45: Fully extended and rotated SODESAL tracking

3.8 Steam Boiler

The design of the SODESAL boiler mimicked the characteristics of a solar water heater system since the copper heat-pipe used for heat exchange is typically inserted into a manifold alongside other heat-pipes. Since the SODESAL system would only use a single heat-pipe, the boiler was designed around the shape of the heat-pipe's condenser bulb. Stainless steel was chosen as the boiler material due to its high corrosion resistance and heat transfer properties. The design for the boiler was simplified to ensure welds were water tight around the manifold and would fit snug around the top of copper heat-pipe bulb. The boiler needed to have a low mass, operate at different system angles and allow for both batch and continuous flow tests.

3.8.1 Boiler Construction

Precise measurements were taken of the copper heat-pipe bulb's diameter and length so that a stainless-steel pipe could be selected for the manifold. The manifold's internal diameter was slightly larger than the outside diameter of the copper heat-pipe bulb. The bulb will expand during operation and tightly press against the inside of the manifold (Figure 3.46)

Figure 3.46: Boiler Manifold Plug with Heat-Pipe Bulb and Thermocouple

A stainless-steel cooking container was used for constructing the main body of the boiler. The cooking container was selected because it had a low mass and relatively low cost. A stainless-steel plate was used to cap off both the top of the manifold plug and seal the bottom of the boiler (Figures 3.47 & 3.48). The components for the stainless-steel boiler were polished using metal grinders and valves were installed for both batch and continuous flow operations (Figure 3.49).

Figure 3.47: Boiler Components

Figure 3.48: Welded Boiler

Figure 3.49: Finished Stainless Steel Boilers with Inlet and Outlet Valves

A heat transfer paste is applied to the surface of the heat-pipe bulb and manifold to increase heat transfer between the two surfaces. Air has poor heat transfer properties and fills the area around the manifold. The thermal paste increases heat transfer by replacing the air with a material between the two surfaces when they are in contact. Excessive heat transfer paste can inhibit heat transfer by acting as an insulator, so a minimal amount of thermal paste is applied. The heat-bulb will expand during operation and press into the manifold; wrapping the heat bulb with pea size drops of thermal paste allows for the material to spread around the surface during operation.

The boiler is wrapped in insulation to reduce heat loses through the external surface of the boiler. An inlet valve is located on one of the sides of the boiler to allow water to enter the boiler for filling and continuous operation. The steam outlet is located at the top of the boiler and can accept a silicon tube for condensation collection (Figure 3.50).

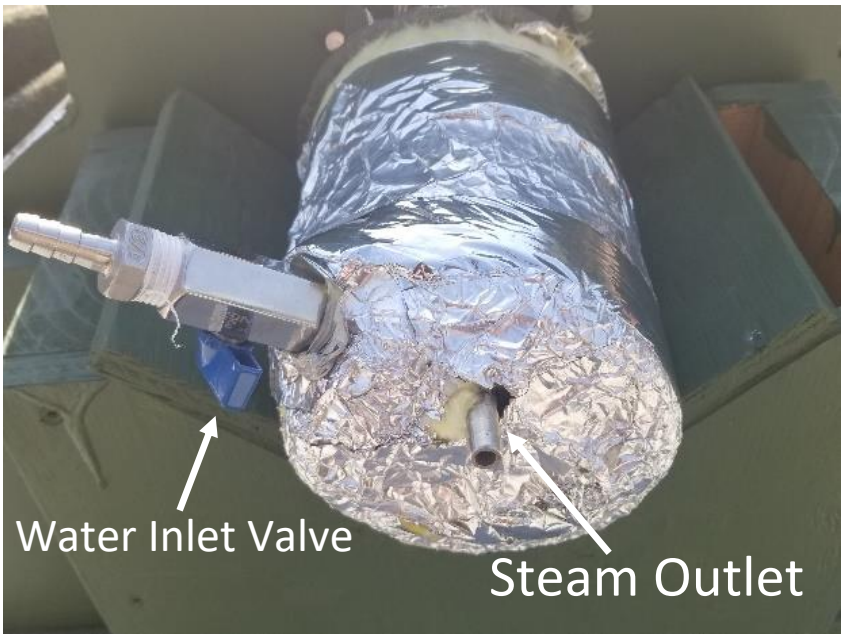

Figure 3.50: Mounted Boiler Wrapped in Insulation

The SODESAL boiler has a brine discharge valve at the bottom of the boiler which also allows for water to recirculate through the boiler during continuous flow operations.

3.8.2 Recirculation Tank and Pump Test

A recirculation test was performed to identify what conditions were possible for a steady-state flow operation when the internal volume of the tank was unknown. The recirculation tank could be used for future tests to aid in cooling the boiler and promote better heat exchange between the boiler manifold and internal copper heat-pipe condenser bulb (Figure 3.61). The

recirculation tank would help simulate a continuous steady-state flow system while recycling the generated heat in the boiler to preheat incoming source water.

Figure 3.51: Recirculation Tank and Boiler Pump Test

Two liters of water were used to initially fill the stainless-steel base tank and was enough water to cover a submersible garden water pump purchased from a local hardware store. An additional liter of water was added to the base tank to maximize volume for operation. The maximum volume for the base tank is 3.5 L. The maximum volume of the boiler was found by closing the bottom valve of the boiler and filling with the pump until overflow. The maximum volume of the boiler is about 1.9 L. The ideal boiler volume is between 1.5 L – 1.75 L, depending on the angle of the boiler, to allow adequate internal space for steam generation.

The submersible water pump was set to the maximum flow which would allow the greatest circulation and identify what the maximum steady-state flow is between the base tank, pump and boiler discharge valve. The boiler discharge valve was used to adjust the boiler volume to find a steady state flow rate.

The flowrate of the pump is about 30 mL/s. This pump rate was found by first closing the bottom valve of the boiler so that only the boiler volume would increase. The pump was turned on for a set amount of time and the volume of water that entered the boiler was measured using a graduated cylinder. Estimated fill time of the boiler for testing was between 50 – 60 seconds assuming no kinks in the silicon tube to impede pump rate. The pump test verified that a recirculation system was practical for future tests using the designed boiler in a continuous flow system. The results of the recirculation pump test are in Table 2.

Table 3: Recirculation Tank and Boiler Pump Test

Pump Time	Volume Measured	Calculated Flowrate
35 seconds	1050 mL	30 mL/s
60 seconds	1750 mL	29.2 mL/S
50 seconds	1480 ml	29.6 mL/s
52 seconds	1560 mL	30 mL/s

3.9 Safety and Mitigation

The SODESAL system's tracking frame required reinforcements and hazard mitigation to safely operate. The frame was painted with a water-resistant stain to reduce the effects from environmental water damage. Protective padding was installed underneath the mirror on the base of the frame so that the collapsible support frames would not damage the wood surface (Figure 3.52).

Figure 3.52: Protective Padding for Collapsed Supports

The frame underneath the top endcap was reinforced with steel telescoping pipes to support the weight of a full boiler and allow for a safe and secure slope adjustment. Several locking mechanisms were required to secure the telescoping pipes and the frame in place when elevated. The steel telescoping pipes each had a lock at the base, one for the telescoping outer channel to prevent the pipes from sliding and a final lockable hinge where the supports connect to the tracking frame (Figures 3.53 & 3.54).

Figure 3.53: Telescoping Lock Mechanism (Bottom)

Figure 3.54: Telescoping Lockable Hinge

Along each side of the tracking frame are supports that lock in place to help displace the combined weight of the parabolic mirror and boiler. The side supports can carry the entire weight of the system and help prevent the system from swaying sideways (Figure 3.55).

Figure 3.55: Tracking Frame Side Supports

The tracking frame presents a fire hazard since the parabolic mirror can burn and ignite the wood frame, even when not elevated and focused. A portion of the top endcap was scorched during storage when sunlight was able to enter through a small hole in the tarp used to cover the SODESAL system (Figure 3.56).

Figure 3.56: Scorched Endcap

The mitigate potential fire hazards, the endcaps were covered in a reflective tape to redirect and disperse concentrated sunlight that may contact the wood surface (Figures 3.57 & 3.58).

Figure 3.57: Bottom Endcap with Reflective Tape Figure 3.58: Top Endcap with Reflective Tape

Additional reflective tape was wrapped around the bottom portion of the PVC cap that holds the evacuated tube in place to prevent the reflected sunlight from damaging the cap further (Figures 3.59).

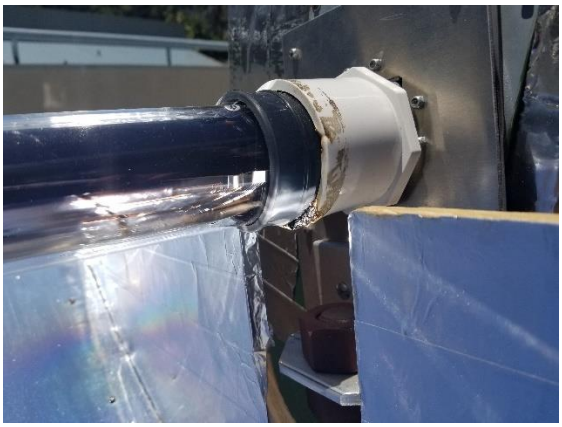

Figure 3.59: Scorched Evacuated Tube Cap (left), Protected Evacuated Tube Cap (right)

A fire blanket was used to cover the parabolic surface during setup, operation and storage to prevent any unwanted sunlight concentration. The testing area was cordoned off with caution tape during operation to protect the operators and public (Figure 3.60). During storage, the SODESAL system is covered in multiple tarps to prevent potential fire hazards due to penetrating sunlight and to protect from rain and other environmental hazards.

Figure 3.60: SODESAL System with Safety Barrier and Fire Blanket

4. PHASE 1: STEAM PRODUCTION

The objective of the Phase 1 experiment was to produce steam using a parabolic trough solar concentrator with an evacuated tube, resembling the experiment by Mosleh at the Sharif University of Technology in Tehran, Iran [25]. This phase was conducted as a proof of concept study to verify that steam production was possible.

4.1 Methodology

The latitude for the Sharif experiment (35.7036 ° N) is very similar to the latitude at the Cal Poly test location (35.3013° N). The latitude was used to set the slope of the PTSC to about 35° [25]. Method 4 tracking was used to track the sun's position since the slope of the mirror was fixed and the tracking frame could easily be moved around a vertical axis to follow the solar azimuth (Figure 4.1).

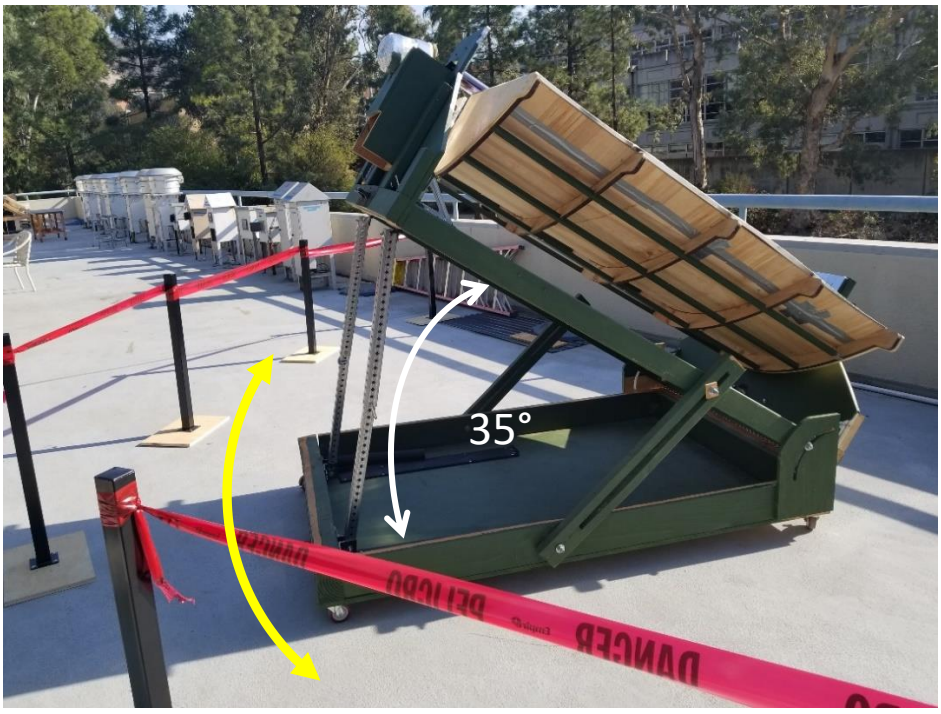

Figure 4.1: Phase 1 Experimental Design - mirror slope (white), sun tracking rotation (yellow)

Approximately 1.5L of tap water was used to fill the boiler before testing. The brine discharge valve and inlet valve on the side of the boiler were closed to simulate a batch operation (Figure 3.54). Once the boiler was filled, the tracking frame was moved into the testing area and rotated every 5 minutes so that the mirror's surface azimuth angle (γ) = the solar azimuth angle (γ_s) as described in Section 3.7.4 for Method 4 tracking.

Direct Normal Irradiation (DNI) and Global Horizontal Irradiation (GHI) were recorded using an Eppley Pyrheliometer and Pyranometer after each adjustment of the mirror (Figures 4.2 & 4.3).

Figure 4.2: Eppley Pyrheliometer

Figure 4.3: Eppley Pyranometer

The Pyrheliometer required realignment for each measurement due to the movement of the sun. The temperature between the copper heat bulb condenser and the inside of the boiler's stainless-steel manifold were recorded manually using a K-type thermocouple and Fluke Multimeter (Figure 3.58).

Figure 4.4: Boiler Thermocouple Position

4.2 Phase 1 Results

During preliminary testing, the experimental design was successful in utilizing concentrated sunlight to boil 1.5 L of tap water in approximately 25 minutes, before the system overheated. The produced steam was collected and condensed in a silicon tube open to the air (Figure 4.5).

Figure 4.5: Steam Condensation Collection

Shortly after reaching boiling temperatures, the copper heat pipe overheated and ruptured, breaking the bottom of the evacuated tube (Figures 4.6 and 4.7). No one was injured.

Figure 4.6: Ruptured Copper Heat Pipe and Aluminum Heat Transfer Fin

Figure 4.7: Broken Evacuated Tube

The solar radiation and boiler temperature data for the copper-heat pipe rupture are shown in Figure 4.8.

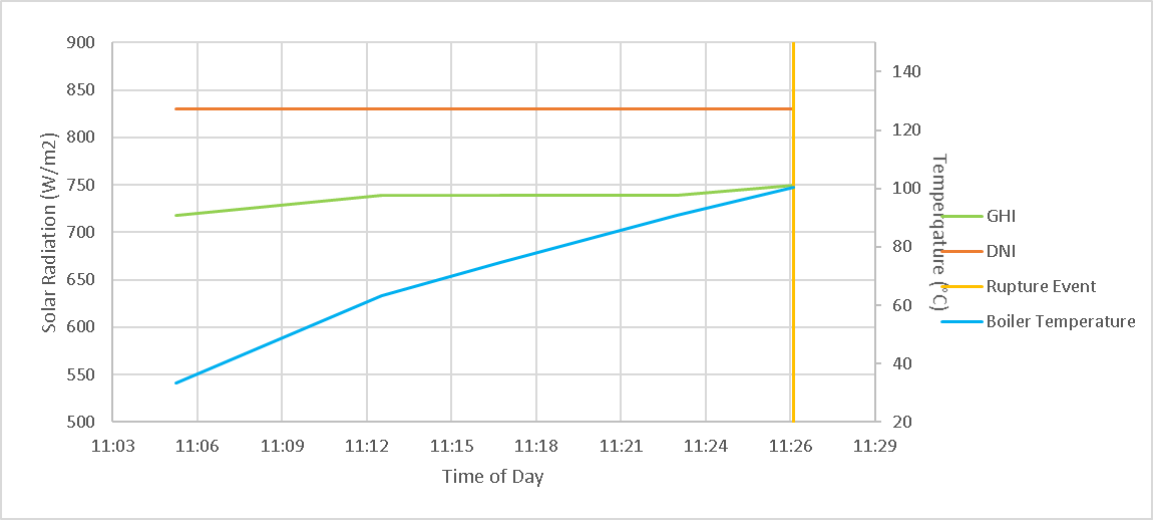

Figure 4.8: Preliminary Phase 1 Test and Rupture Event

4.3 Phase 1 Implications

The suspected cause of the rupture was a buildup of pressure caused by inadequate heat transfer between the copper heat-pipe condensing bulb and the stainless-steel manifold in the boiler. The internal walls of the copper heat pipe were relatively thin, about 1-2mm, and were unable to contain the internal pressure from the rapid expansion of the water/glycol heat transfer fluid mixture during concentration.

During future tests, the evacuated tube should be filled with an oil or other liquid with a boiling point higher than water. Filling the evacuated tube with a liquid was avoided initially due to the risk that the glass tube could shatter from moving the mirror for tracking or uneven heating. However, the addition of a fluid could allow more energy to transfer out of the copper heat pipe and mitigate against a rapid expansion of the water/glycol heat transfer fluid [25].

5. PHASE 2: TEMPERTURE DISTRIBUTION OF AHTF

Analysis of the Phase 1 experiment indicated that additional testing was required to understand how thermal energy is distributed across the inside of the evacuated tube during solar concentration. Since the copper heat-pipe posed a risk of rupturing due to overheating it was removed from the aluminum heat transfer fin (AHTF). The AHTF is the first material that contacts the surface of the evacuated tube's inner glass wall, so it was decided that measuring the lateral heat distribution across the AHTF would safely represent the internal temperatures during solar concentration. Measuring the AHTF's lateral heat distribution would help aid in determining which materials could be selected for a future safe and effective heat transfer system, and potentially help model thermal outputs for steam production.

5.1 Phase 2 Experimental Design

The lateral heat distribution for the AHTF was measured with three high-temperature K-type thermocouples capable of accurate measurements up to 1200° C. The thermocouples were secured to the inside of the AHTF using Kapton thermocouple tape which is capable of handling high temperature applications (Figures 5.1 & 5.2).

Figure 5.1: Aluminum Heat Transfer Fin and Thermocouples

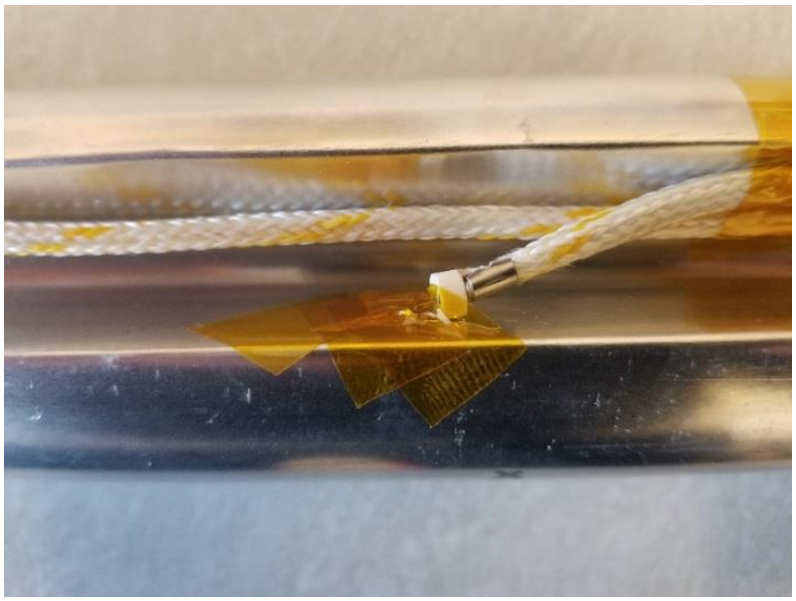

Figure 5.2: Thermocouple Placement with Kapton Tape

The position of each thermocouple in relation to the evacuated tube in the parabolic trough solar collector is shown in Figure 5.3.

Figure 5.3: Thermocouple Locations for Lateral Heat Distribution Collection

The channel 1 (CH1) thermocouple was placed at the location where the edge of the collector's aperture lines up with the evacuated tube. About 130 mm of the evacuated tube's open end extends past the PTSC's aperture edge and therefore does not receive concentrated sunlight (Figures 5.4 & 5.5).

Figure 5.4: Evacuated Tube Extension & CH1 Location

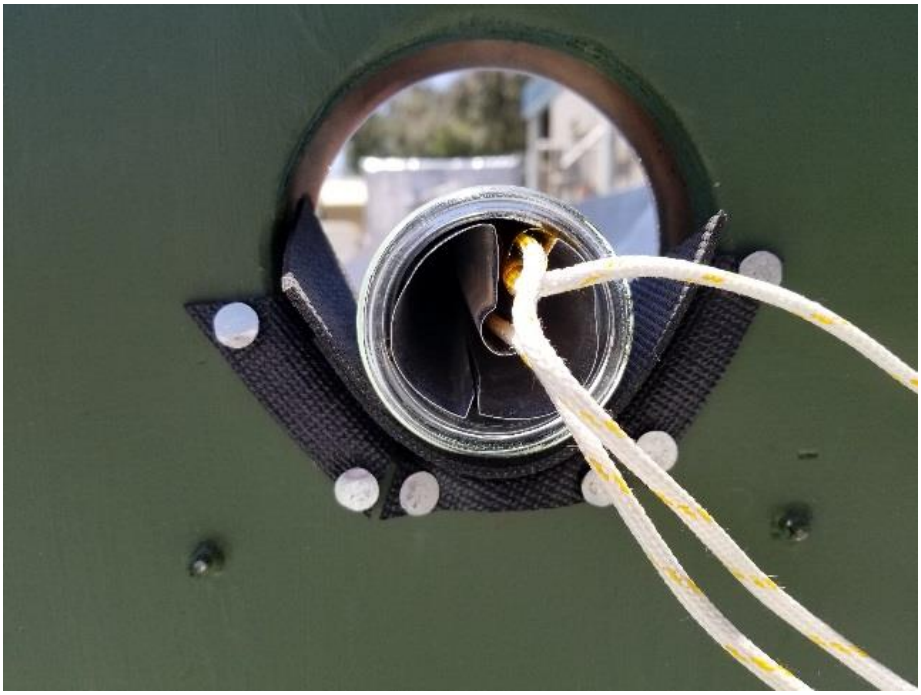

Figure 5.5: Open End of Evacuated Tube

Channel 2 (CH2) represents the center of the AHTF, and Channel 3 (CH3) is the location where the copper heat pipe ruptured during the Phase 1 experiment. CH2 and CH3 are located approximately 86.4 cm and 152.4 cm, respectively, from the open end of the evacuated tube. Thermocouple temperature data was collected automatically each second for 6 hours using a LabQuest® 2 data logger. The data logger was set to run 3 hours before and after solar noon to measure the temperature on the AHTF during the portion of the day with the highest solar radiation.

Method 1 tracking was used for the Phase 2 experiment due to the simplicity of setup for operation. The tracking frame was aligned parallel to the E-W axis and the slope of the mirror was set to align with the sun at solar noon (Figure 5.6).

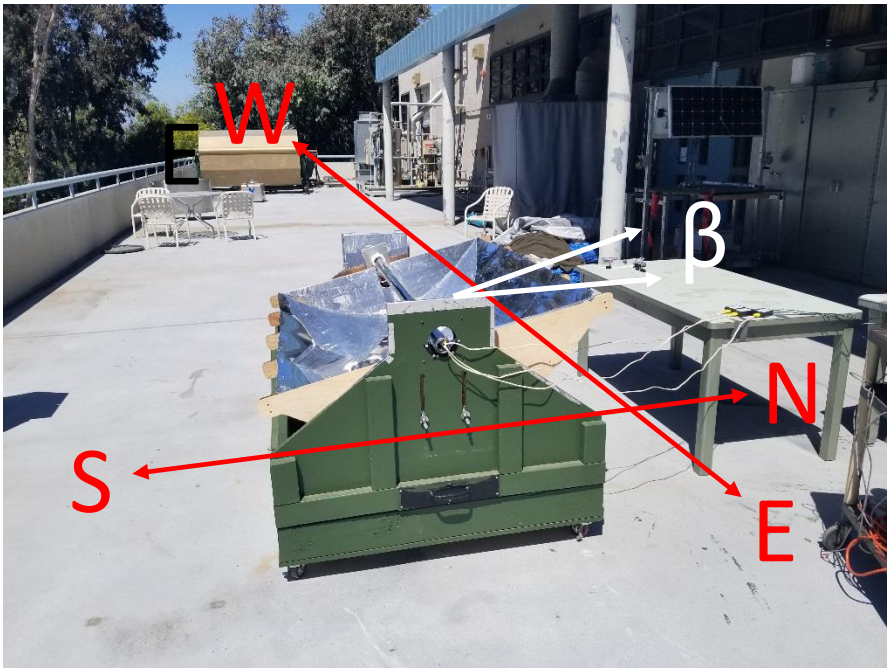

Figure 5.6: Phase 2 Method 1 Alignment and Slope

The PTSC was rotated using an electric motor and Arduino power switch so that the mirror would align with the sun at the appropriate slope angle (β) for solar noon (Figure 5.7).

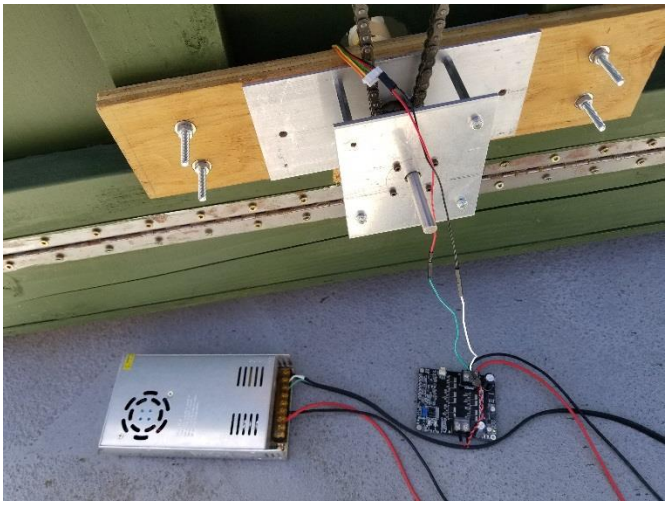

Figure 5.7: Tracker Electric Motor and Arduino Power Switch

Sunlight data was collected using a LabQuest® 2 data logger connected to an Eppley pyrheliometer and pyranometer. The solar radiation sampling window was set to 5 minutes for the 6-hour duration of the test.

5.2 Phase 2 Results

Solar radiation and aluminum heat transfer fin temperatures were measured over several days, and representative data for the AHTF's heat dispersion are shown in (Figure 5.8). The graph shows the time of day for solar noon as a reference for the middle of the experiment's duration. The collected Global Horizontal Irradiation (GHI) shows the gradual change in sunlight throughout the morning until reaching a climax at solar noon and descending at relatively the same rate during the afternoon. Direct Normal Irradiation (DNI) fluctuates throughout the day depending on weather conditions and how clear the sky is above the collector. Since the

collector only uses DNI for concentration, this value is of importance when calculating the power output (P) of the system.

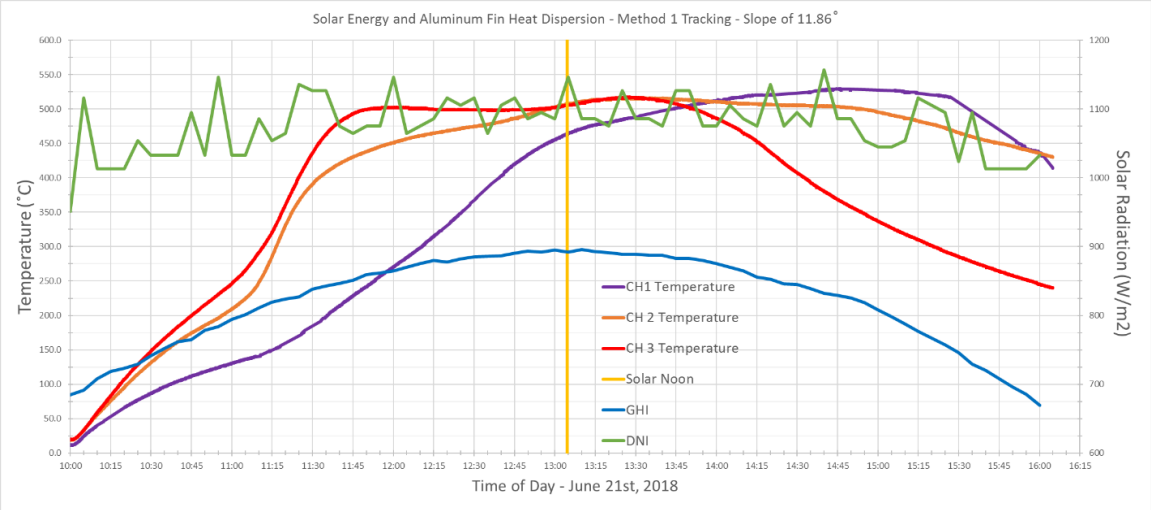

Figure 5.8: Aluminum Fin Heat Dispersion and Solar Energy for Summer Solstice

The observed changes in lateral heat distribution are a result of using Method 1 tracking. Since Method 1 tracking requires a single adjustment to align the mirror at solar noon, the AHTF will experience different timelines of rapid heating and cooling. The maximum temperature achieved on the AHTF was about 525°C located at CH1 after about 5 hours of heating. The operational temperature of the PTSC and AHTF is about 500°C for all channels once proper alignment is achieved.

During the morning, the angle of incidence (θ) onto the evacuated tube is such that CH1 is shaded and encounters a delayed and slower rate of heating (Figure 5.9). As the day continues, the angle of incidence (θ) approaches near 0° at solar noon which is represented by the maximum temperatures seen for Channels 2 and 3 (Figure 5.8).

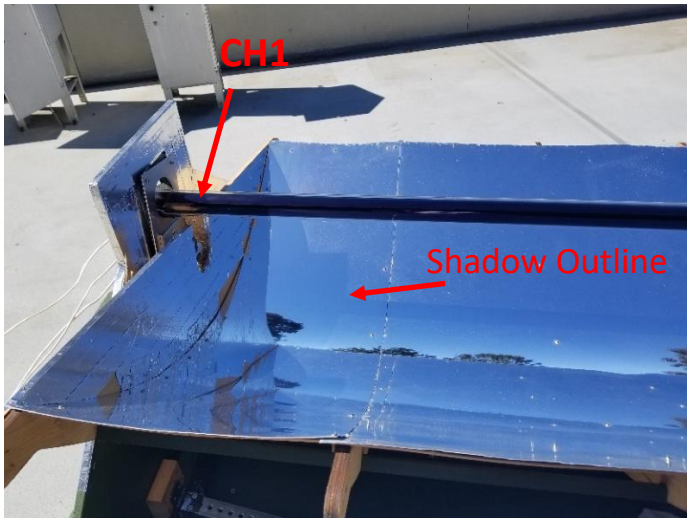

Figure 5.9: CH1 Shading by System Frame before Solar Noon.

CH2 and CH3 measurements are elevated compared to CH1 because both sensors receive constant sunlight throughout testing until the afternoon (around 13:45 PM) when the temperatures begin to drop due to increased shading from the system's frame and an increased angle of incidence on the opposite end of the evacuated tube indicated by the CH3 location (Figure 5.10).

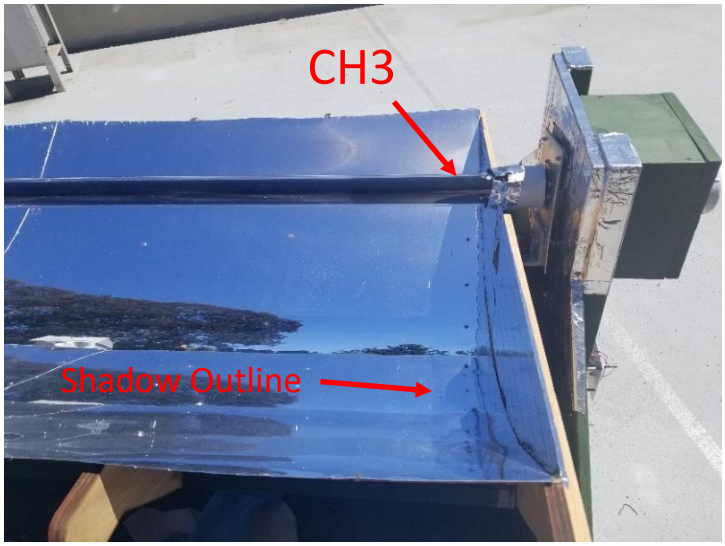

Figure 5.10: CH3 Shading by System Frame after Solar Noon.

CH1 has the highest measured value in the afternoon around 14:45 PM. The reason for CH1's high temperature value is due to the alignment of the sun and the duration of heating located at CH1 during operation. Although CH1 does not receive direct sunlight until later in the experiment, the location is still heating up due to the lateral heat transfer across the AHTF. After solar noon, CH1 continues to receive angled sunlight whereas CH3 begins to rapidly cool due to shading.

5.2.1 - Power Output and Theoretical Maximum Freshwater Yield

The total output of steam is dependent upon the surface area of the collector and the combined thermal efficiency of the PTSC and heat transfer system. The power output (P) of the PTSC can be estimated using Equation 28 where (S) is the average DNI (W/m^2) over the operating period, (A_a) is the total aperture area (m^2), (α_r) is the specular reflectance of the collector surface (%), and (t) the total time of operation (hours) [3].

Equation 28: CSP Power Output

$$P = (S)(A_a)\left(\frac{\alpha_r}{100}\right)(t)$$

The maximum theoretical freshwater yield (V_{TMax}) in (L/m^2·hr) can be calculated using Equation 29 where (P) is the power output (kWh) of the CSP, (T_{bp}) is the boiling temperature (°C) of pure water at 1 atm, (T_{amb}) is the ambient temperature (°C), (C_p) is the heat capacity (*4.184 J/kg·°C)* of water, (H_v) is the latent heat of vaporization (kJ/kg) of pure water at 1 atm and (ρ) the density of water (kg/m^3) at 1 atm and ambient temperature [3].

Equation 29: Maximum Theoretical Freshwater Yield

$$V_{TMax} = \left(\frac{P}{\rho\left((T_{BP}-T_{amb})(C_P)+(H_v)\right)}\right)\left(\frac{3600s}{1hr}\right)\left(\frac{1}{A_a}\right)$$

The maximum theoretical freshwater yield for the SODESAL system using the above-mentioned conditions and average DNI of the summer solstice is 1.42 $L/m^2 \cdot hr$. This value does not represent the actual output of the SODESAL system since the theoretical freshwater yield is assuming 100% thermal conversion of solar radiation into steam production.

Actual freshwater yield calculation would need to account for thermal losses associated with heat transfer between the aluminum heat transfer fin, heat exchange fluid and transfer system, steam generator and condenser. Similar small-scale systems have achieved system thermal efficiencies between 22.1 – 65.2% when producing steam for direct distillation [25]. If the mentioned efficiency for an evacuated tube with only an AHTF is applied to the SODESAL system, the adjusted theoretical freshwater yield becomes 0.31 $L/m^2 \cdot hr$.

5.2.2 - Summer Solstice vs Winter Solstice Solar Radiation Potential

Solar radiation data was collected for both the winter and summer solstices to compare the theoretical maximum and minimum values for available solar energy for the Cal Poly test location (Figure 5.11). The summer and winter solstice measurements demonstrate the maximum and minimum available solar radiation throughout the year.

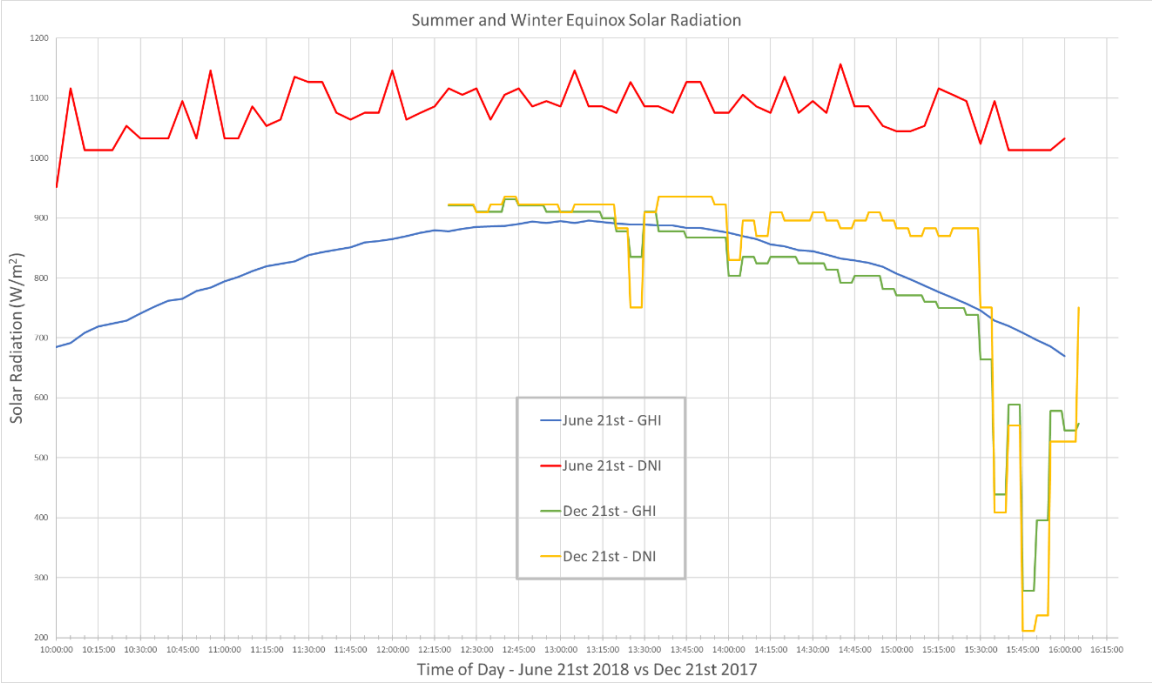

Figure 5.11: Summer 2018 vs. Winter 2018 Solstice Solar Radiation for Cal Poly Test Location

The GHI values were similar for both sampling days, whereas the DNI measurements indicate significant differences in atmospheric conditions. During the summer when DNI is highest the angle between the sun and the collector is lowest, resulting in longer days and less atmosphere to absorb and scatter direct solar radiation [3]. During the winter when DNI is lowest, the angle between the sun and the collector is highest, resulting in shorter days and more relative atmosphere to absorb and scatter direct solar radiation. The dramatic drops in the winter solstice solar radiation measurements were due to clouds blocking sunlight to the collector's surface.

On the winter solstice (Dec 21st), the sun's incident radiation is impeded the most by the earth's atmosphere due to the sun's low position in the sky [3]. The winter solstice DNI measurements can help quantify a theoretical minimum freshwater yield for the SODESAL system since these measurements represent the lowest potential solar radiation for the location. Assuming 100%

thermal efficiency and using an average winter solstice DNI of 831 W/m^2, the theoretical minimum freshwater yield is 1.16 L/m^2·hr. The adjusted minimum freshwater yield using the thermal efficiencies from Mosleh [25] is 0.24 L/m^2·hr.

5.2.3 - Localized Impacts on Solar Thermal Energy

Atmospheric conditions can significantly hinder a CSP system's output if direct solar radiation is blocked by clouds. Cloud coverage blocking available solar radiation and altering the heat distribution of the AHTF was observed for one of the testing days and is shown in Figure (5.12).

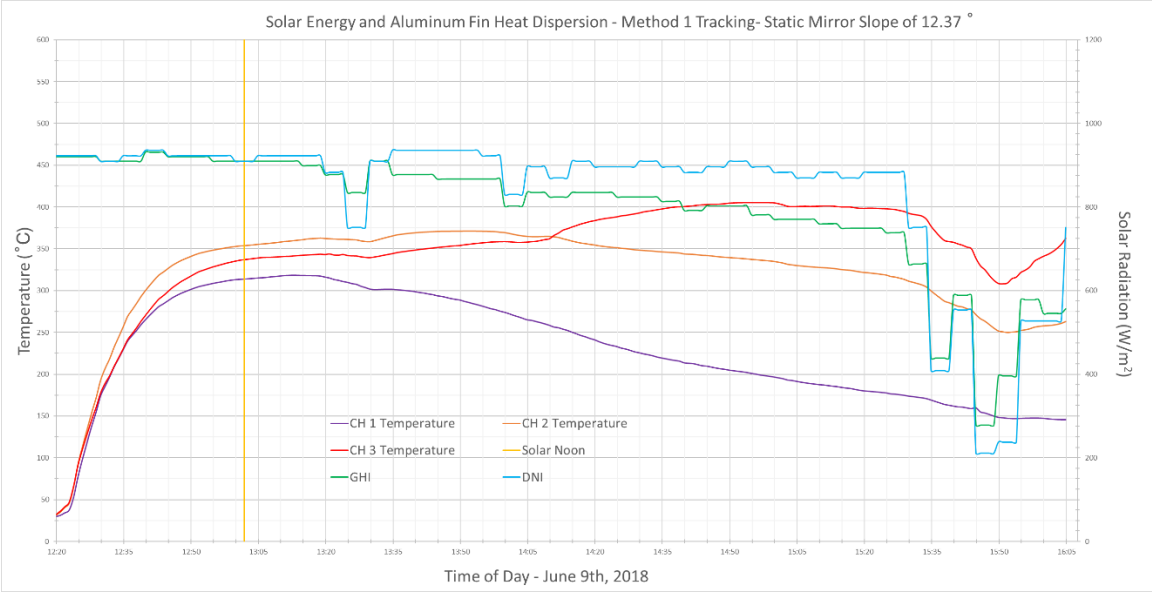

Figure 5.12: Solar Energy and AHTF Heat Dispersion for Cloudy Day

As the solar radiation increased, the temperatures for Channels 2 and 3 began to climb while Channel 1's temperature plateaued and declined. At around solar noon, the temperatures for all 3 channels were relatively consistent indicating an operation window of consistent sunlight. At

approximately 15:30 PM, cloud coverage over the collector peaked, causing the measured solar radiation to plummet along with the temperatures measured inside the evacuated tube. Shading and cloud coverage can significantly reduce the solar radiation received for a PTSC and therefore the freshwater yield for a small-scale solar desalination system. The highest DNI recorded for June 9th was 935 W/m^2 and the lowest value after cloud shading was 211 W/m^2. The effect of cloud shading could therefore reduce the maximum theoretical freshwater yield by up to 77%. The resulting freshwater yield per unit area of collector would drop from 1.23 L/m^2·hr to 0.28 L/m^2·hr.

5.3 Phase 2 Implications

The Phase 2 experiment demonstrated the importance of alignment for providing consistent thermal energy to a small-scale CSP system. The lateral heat distribution across the aluminum heat transfer fin varies throughout the day depending on the total time of ideal solar alignment and the angle of incidence with direct solar radiation (θ). Method 1 tracking was used as a simple way to align a parabolic trough solar collector with solar noon. However, if Method 2 or Method 3 tracking were used to continuously adjust the slope (β) of the collector, the angle of incidence will be minimized during operation. Minimizing the angle of incidence should allow the AHTF to achieve consistent operating temperatures earlier and longer during operation.

Alignment along the polar axis and continuous tracking are two ways to minimize the incident angle (θ) and shading that can occur on the collector or the evacuated tube surface. Shading can provide a significant decrease in solar energy production. A remedy for shading on small-scale systems is to align the tracking frame along the polar N-S axis for continuous tracking operation. N-S tracking with continuous adjustment should reduce the effect of shading from a collector's

endcaps since the incident angle will be less severe for that specific alignment [3]. If the endcap surface area is kept to a minimum, shading will have a minimal effect on N-S axis continuous tracking CSP systems.

6. CONCLUSIONS

This study demonstrated that the SODESAL system can achieve results like other CSP systems. The AHTF used in this SODESAL system achieved temperatures (350 – 525 °C) that are like operating temperatures achieved by large-scale systems (300 - 550°C) [15]. Previous experiments have shown that it is possible to achieve an actual freshwater yield of up to 0.78 $L/m^2 \cdot hr$ with an operating cost of $\$ 0.0450/l/m^2$ [25]. This SODESAL system can reach boiling for 1.5 L of water in approximately 25 minutes, however the copper heat-pipe used for heat exchange ruptured from overheating. Small-scale CSP systems are limited by the thermal efficiency of the heat exchange system. Method 4 tracking was utilized to provide the necessary angle to allow the copper heat-pipe to circulate the internal heat transfer fluid, however, a horizontal alignment using Methods 1, 2 or 3 could utilize a more robust heat transfer loop that is safer and more effective. The lateral heat distribution of the AHTF is dependent upon the PTSC's solar incident angle. A consistent lateral heat distribution occurred across the AHTF approximately 40 mins after solar noon. The temperature difference between each end of the AHTF can exceed over 225 °C leading up to and following solar noon when the PTSC was set at a static slope.

Large-scale CSP systems have the benefit of operating multiple PTSCs in an array to maintain consistent heating of a heat transfer fluid throughout a full sunlight day. Longer PTSC's thermal efficiencies are less affected by endcap shading due a higher proportion of reflector surface area exposed to sunlight compared to small PTSCs. The SODESAL system described herein was affected by shading due to structural design flaws and the chosen method of tracking which limited the timeline of consistent maximum operating temperatures. Based on these findings

this SODESAL system has the potential for future applications, system improvements and additional research.

6.1 Small-Scale CSP Applications

Combined CSP and Seawater Reverse Osmosis (SWRO) systems are commonly used in areas with abundant sunlight to provide freshwater to water-scarce regions [15, 19, 20]. However, these systems require economical infrastructure and consistent sources of solar thermal energy to be competitive with fossil-fuel powered systems. Small-scale CSP desalination systems have the potential to produce steam for both power generation and direct steam distillation on a scale that can be more affordable for off-grid applications and non-conventional source waters for treatment [20, 23, 24, 25].

Aside from seawater desalination, small-scale CSP systems could also be implemented to recycle wastewaters in areas that do not have the infrastructure or space available for commercial size systems. Small-scale CSP systems could be used to treat agricultural run-off, fracking wastewater or even provide on-demand solar power and water treatment for disaster relief zones [20, 22]. The size of small-scale systems could serve as a pilot to test the requirements and model a larger scale system at minimal capital costs.

6.2 Future Studies

Small-scale solar desalination systems have been proven to provide solar thermal outputs comparative to large-scale CSP desalinations systems [25, 24, 25]. Additional research must be made to maximize the thermal efficiency, reduce the capital costs and increase the longevity of small-scale systems. Improvements in the freshwater yield per unit of collector area are of

importance for small-scale systems vying to reduce the relative cost of producing steam. With some improvements to the SODESAL system design, additional studies using this system may allow for even greater insight into the potential for small scale solar desalination systems.

6.2.1 Structural Improvements

The solar desalination system shown herein was constructed as a prototype to understand the process of manufacturing and the capabilities of a small-scale CSP system. Over a year of operation has caused many parts of the SODESAL system to warp, crack or even break from the stresses of operation.

Warping of the collector's rib structure can alter the mirror's reflected image and reduce the effectiveness of reflectivity or create unwanted concentration. Sunlight concentration spots must be mitigated on the structure if wood is used since wood can combust under concentrated sunlight. Reflective tape was used as a quick way to fix concentration spots that are causing the structure system to overheat, but aluminum is recommended for the structure due to its light weight, strength, manufacturability and high melting point. Aluminum should replace the wooden structure of the tracking frame so that the system is reinforced, and the weight of the collection system is supported.

A robust motor, gear and tracking system is necessary to maximize collection of solar radiation into the collector. The gear system and ball bearing mount used for tracking needs to be reinforced to prevent flexing and subsequent damage while a force is acted upon it during rotation. Some of the ball bearings popped out of the mount due to excessive flexing of the structure.

The length of the collector is limited by the length of the evacuated tube. The structure supporting the evacuated tube should not impede or block sunlight entering the collector. The endcaps used in the system described herein, although structurally necessary, could be changed to allow for sunlight to pass through if stronger materials are used to occupy less space.

The evacuated tube is constructed out of a borosilicate material and therefore has the potential to break under shocks or impacts. Alternative materials that provide the same thermal conditions and sunlight transmission should be investigated to provide more robust solutions to solar radiation conversion to thermal energy.

The copper heat-pipe used in this SODESAL system ruptured due to overheating from inadequate heat exchange between the condensation bulb and steam generator. A pressure relief valve could mitigate this risk if the mechanism for heat transfer is not compromised. The addition of a heat transfer paste can also improve heat exchange between the heat-pipe bulb and boiler when both are in direct contact.

6.2.2 Operation Improvements

Implementing Methods 2 and 3 for continuous tracking should improve the duration of maximum operating temperatures for this SODESAL system. A longer duration of maximum operating temperature will provide a more consistent heat transfer which is critical to maintaining a constant production for steam for either energy production or desalination.

A steady-state flow of feed water through the boiler could limit the risk of the copper heat-pipe from overheating since a consistent flow of cooler water will provide better heat exchange for steam production compared to a batch-reactor with stagnant hot water.

A heat exchange fluid that is pumped and looped through the evacuated tube to exchange heat through an external steam generator could greatly improve the thermal efficiency and safety of the SODESAL system. This type of heat exchange system would better simulate large-scale CSP systems and allow for additional methods of tracking that do not require a minimum PTSC slope for internal heat exchange like in Method 4 tracking.

6.2.3 Additional Experiments

The addition of a medium inside the evacuated tube has shown to substantially increase the thermal efficiency and freshwater yield of other small-scale systems [25]. The evacuated tube for the SODESAL system should be filled with a medium like oil, or a solid medium like sand that has a higher boiling point than water. Sand is a readily available solid medium that could be added to the inside of an evacuated tube to help evenly distribute heat across the AHTF and heat transfer system during operation. The internal medium may also provide heat storage and increase the duration of solar thermal production during off-peak hours when solar radiation is limited, like how molten salt is used as thermal storage in solar tower power systems [13].

The size of a small-scale CSP system provides the benefit of being able to compare different tracking methods to identify the best solution for a location. A thermal output test like the one performed for Phase 2 at different orientations could satisfy a comparative test to see if the

window of operational temperature can be extended for different tracking methods.

A heat transfer system that can withstand high internal temperatures and pressure should be implemented with a simple distillation and condensation system to test the capabilities for small-scale desalination. Once a small-scale system is constructed that is durable and thermally consistent with converting solar thermal energy for steam production a model of the system should be developed to predict performance for different source waters. Different source waters should be tested to identify what constituents if any are transferred through the separation process.

A study should be done for a small-scale CSP system's capability to produce solar thermal energy for heat storage. Surplus thermal energy not used for steam generation could be used to charge a heat storage, prolonging the window of operation during times of insufficient solar radiation [20]. Excess thermal energy could also be recycled to preheat source water going into the CSP system, effectively increasing the thermal efficiency [22].

An optimization of a small-scale array system should be conducted to determine what the maximum thermal performance is for a given length of evacuated tube. At a certain point a PTSC cannot be made any wider since the width would impede with the tracking motion; an array of small-systems could be more economical than fewer large-systems if space is limited for the location of the system.

A study verifying modeled results against measured results should be conducted for small-scale CSP systems to predict thermal efficiencies and expected steam generation yields. Researchers

at the University of Engineering and Technology in Karachi, Pakistan developed a probabilistic model for a Parabolic Trough Concentrator (PTC) to determine a single correlation for outlet temperature of Syltherm 800, a commonly-used heat transfer fluid (HTF).

The model was able to identify several input factors that had an insignificant effect on the modeled thermal performance of a PTC including the diameter of the absorber pipe, the thickness of the evacuated tube's glass envelope, the spacing between the absorber pipe and glass envelope, the emissivity of the absorber pipe, the optical efficiency, ambient temperatures and wind speed. The model was able to explain 98.4% of the variability in the heat transfer fluid outlet temperatures. The methodology used in Pakistan could be applied to find correlations for other output parameters of PTCs using this SODESAL equipment.

REFERENCES

[1] Shiklomanov, I. “World Fresh Water Resources.” Water in Crisis: A Guide to the World’s Fresh Water Resources, edited by Peter H. Gleick, Oxford University Press, New York, 1993. Accessed from: https://water.usgs.gov/edu/earthwherewater.html

[2] Hoekstra, A.Y. “Water Footprints of Nations: Water Use by People as a Function of Their Consumption Pattern.” Integrated Assessment of Water Resources and Global Change A North-South Analysis, 2007, pp. 35–48.

[3] Duffie, John A., and William A. Beckman. “Solar Engineering of Thermal Processes.” 4th ed., Wiley, 2013.

[4] Vashishtha S. “Differentiate Between the DNI, DHI and GHI?” First Green Consulting. 26 April, 2012. https://firstgreenconsulting.wordpress.com/2012/04/26/differentiate-between-the-dni-dhi-and-ghi/

[5] Solargis. “Direct Normal Irradiation.” Solar Resource Maps of World. The World Bank, 2017. https://solargis.com/maps-and-gis-data/download/world

[6] Solargis. “Direct Normal Irradiation - United States of America.” Solar Resource Maps of USA. The World Bank, 2018. https://solargis.com/maps-and-gis-data/download/usa

[7] Solar Prospector. “National Solar Radiation Database Data Viewer.” Interactive Mapping Tools. NREL. 2015. https://maps.nrel.gov/nsrdb-viewer

[8] Solargis. “Global Horizontal Irradiation.” Solar Resource Maps of World. The World Bank, 2017. https://solargis.com/maps-and-gis-data/download/world

[9] Solargis. “Global Horizontal Irradiation – United States of America.” Solar Resource Maps of USA. The World Bank, 2018. https://solargis.com/maps-and-gis-data/download/usa

[10] Aden B Meinel and Marjorie P. Meilen. “Applied Solar Energy, An Introduction.” Addison Wesley Publishing Company, Inc. Philippines, third edition edition, 1976

[11] LandArtGenerator, “The 19th Century Solar Engines of Augustin Mouchot, Abel Pifre, and John Ericsson.” 29, February 2012. http://landartgenerator.org/blagi/archives/2004

[12] “Concentrating Solar Power (CSP) Technologies” Utility-Scale Solar Energy. Solar Energy Development Programmatic EIS, 2018. http://solareis.anl.gov/guide/solar/csp/

[13] Brown, P. “Spain’s Solar Salt Open Door to 24-7 Clean Electricity” Energy. Climate Home News. 5, January 2014. http://www.climatechangenews.com/2014/05/01/spains-solar-salt-opens-door-to-24-7-clean-electricity/

[14] Sawin, Janet L., and Eric Martinot. "Renewables Bounced Back in 2010." Renewable Energy World, 29 Sept. 2011. http://www.renewableenergyworld.com/rea/news/article/2011/09/renewables-bounced-back-in-2010-finds-ren21-global-report

[15] Trieb, F., et al. "Technologies for large scale seawater desalination using concentrated solar radiation." Desalination, 235, 2009, pp. 33-43.

[16] Ghaffour, N., et al. “Technical review and evaluation of the economics of water desalination: current and future challenges for better water supply sustainability.” Desalination, 309, 2013, pp. 1997-207

[17] “Global Desalination Capacity Growing Substantially, Finds Study.” WaterWorld, 14 October, 2013. https://www.waterworld.com/articles/2013/10/global-desalination-capacity-tops-80-million-cubic-meters-per-day.html

[18] “Desalination Project Forges ahead in California.” Reuters, 10 December, 2009. https://www.reuters.com/article/desalination-california/desalination-project-forges-ahead-in-california-idUSN1021341120091211

[19] Banat, F., et al. "Performance evaluation of the “large SMADES” autonomous desalination solar-driven membrane distillation plant in Aqaba, Jordan." Desalination, 217, 2007, pp. 17-28.

[20] Lienhard, J. H., et al. "Solar Desalination." Annual Review of Heat Transfer, 15, 2012, pp. 277-347. http://web.mit.edu/lienhard/www/papers/reviews/Solar_Desalination_AnnRevHeatTransfer-Vol15-2012-4659.pdf

[21] Voutchkov, N. “Desalination – Past, Present and Future.” International Water Association. 17 August, 2016. http://www.iwa-network.org/desalination-past-present-future/

[22] Stuber, Matthew D. “Pilot Demonstration of Concentrated Solar-Powered Desalination of Subsurface Agricultural Drainage Water and Other Brackish Groundwater Sources.” Desalination, vol. 355, 2015, pp. 186–196.

[23] Leonard, Scott. “A Low Cost Portable Parabolic Solar Concentrator for Combined Heat and Power.” 2012 North American Power Symposium, 2012, pp. 1-6

[24] Newton, C. C., “A Concentrated Solar Thermal Energy System”. Department of Mechanical Engineering. Electronic Theses, Treatises and Dissertations, Florida State University, Paper 2631.

[25] Mosleh, H. J., et al. “A new desalination system using a combination of heat pipe, evacuated tube and parabolic trough collector.” Energy Conversion and Management, vol. 99, 15 July, 2015, pp141-150.

[26] Uzair, Muhammad. “Probabilistic Approach for Estimating Heat Fluid Exit Temperature Correlation in a Linear Parabolic Trough Solar Collector.” Journal of Mechanical Science and Technology, vol. 32, no. 1, 2018, pp. 447–453

[27] “Evacuated Tube and Heat Pipe” Evacuated Tube Solar Collectors. (n.d.). Retrieved from http://www.apricus.com/html/solar_collector.htm#.WvKCG4gvyUk

[28] “24 mm Condenser Copper Heat Pipe Solar Thermal Collector with Aluminum Alloy Frame Working Principle” Heat Pipe Solar Collector. (n.d.). Retrieved from http://www.solarheatercollector.com/sale-8551090-silver-heat-pipe-solar-collector-24mm-condenser-copper-45-degree-angle.html

[29] “Evacuated Tube Heat Pipe Manifold” Red Circle Solar. (n.d). Retrieved from http://www.redcirclesolar.com.au/

[30] “Evacuated Tube Design” Evacuated Tubes. (n.d.). Retrieved from http://www.apricus.com/html/evacuated_tubes.htm#.WvtVwaQvxhE

[31] “Parabolic Trough Reflector” Alternative Energy Tutorials. (n.d.). Retrieved from http://www.alternative-energy-tutorials.com/solar-hot-water/parabolic-trough-reflector.html

[32] “Pool Heating 2” George’s Workshop. 23 August, 2015. Retrieved from https://georgesworkshop.blogspot.com/2015/08/pool-heating-2.html

[33] “Morocco Unveils A Massive Solar Power Plant in the Sahard” International. NPR, 4 February, 2016. Retrieved from https://www.npr.org/sections/thetwo-

way/2016/02/04/465568055/morocco-unveils-a-massive-solar-power-plant-in-the-sahara

[34] Nimerfro, K. “Parabolic Trough Solar Concentrator” Wolfram Demonstrations Project, 13 July, 2009. http://demonstrations.wolfram.com/ParabolicTroughSolarConcentrator/

[35] “ReflecTech Mirror Film” SkyFuel, 2017. Retrieved from: http://www.skyfuel.com/wp-content/uploads/Brochure-SF-ReflecTech_EN.pdf

[36] “NOAA Solar Calculator” [Earth System Research Laboratory, Global Monitoring Division. (n.d). Retrieved from https://www.esrl.noaa.gov/gmd/grad/solcalc/

[37] “Introduction of Nuclear Desalination – A Guide Book” Technical Reports Series No. 400, International Atomic Energy Agency, Vienna, 2000